Meteorology and Atmospheric Physics (2019) 131:1577–1604
https://doi.org/10.1007/s00703-019-0659-0

ORIGINAL PAPER

Diurnal variability of convection over northwest Indian subcontinent observed by the Doppler weather radar data

Soma Sen Roy[1] · Subhendu Brata Saha[1] · S. K. Roy Bhowmik[1] · P. K. Kundu[2]

Received: 7 January 2018 / Accepted: 18 January 2019 / Published online: 6 February 2019

Abstract
The diurnal cycle of convection over a sub-tropical semi-arid inland station—Delhi—has been analyzed in this study based on three different rainfall episodes. Two of these cases represent convection in association with low precipitable water content (< 40 mm) and moderate vertical wind shear (between 4 and 10 m/s) while the third case represents convection under high precipitable water content (> 60 mm) and low vertical wind shear (< 2 m/s). It has been noted that for all the three cases, convection was initiated during the morning hours in the form of single cells, which evolved into multi-cellular convection zones later on those days. The most common mesoscale organization of the clouds in all the three cases had been in the form of convective lines which moved along the mean steering flow in the lower troposphere. However, for case 1, squall line formation and movement were observed during a period of 6 h, which was aided by the high unidirectional shear in the lower-to-middle troposphere, that was absent in other cases. These squall lines were associated with severe surface winds. The convection zones were found to be short lived with less stratiform outflow for case 1, more stratiform outflow for case 2 and longest lifetimes and most stratiform outflow for case 3. This study also indicates that the primary peak of convection and associated rainfall over the region, irrespective of the season, is in the afternoon hours between 1730 Indian Standard Time (IST) and 2030 IST, and lags the diurnal temperature maximum (around 1430 IST) by 3–5 h. When there is sufficient moisture in the atmosphere and convection persists throughout the entire diurnal cycle, a second peak in convection and associated rainfall appears over the region in the early morning hours (between 0230 and 0530 IST). This night time-early morning peak has a greater fraction of stratiform clouds at the beginning of a rainfall episode. As the moisture build up in the atmosphere on day 2 and later of a long-lived episode, new convection was initiated in the night time with increase in the night time rainfall intensity. This implies that pre-monsoon convection over Delhi in the presence of low moisture is primarily unimodal, characterized by short bursts of intense convection with narrow and short-lived cells. Monsoon convection on the other hand, is essentially bimodal, with the early morning peak, often pre-dominating over the afternoon peak and characterized by longer lived cells which are less intense than cells of the pre-monsoon weather systems.

1 Introduction

The spatial and temporal variations of moist convection are a field of increasing interest, especially as the resolution of numerical models is increasing and focus on the cloud resolving scale of numerical models. A major problem in the present day numerical models arises from the lack of accurate simulation of the energy and water cycles (Giorgi and Mearns 1999). The presence of clouds and resulting precipitation is the primary control on these cycles. The lack of accurate representation of these clouds and precipitation processes in numerical models leads to inaccurate model estimation of radiative fluxes and global radiation budget (Trenberth et al. 2009; Trenberth and Fasullo 2010) which further leads to inaccurate representation of the space–time variability of tropical convection in the forecast field (Randall et al. 2003). Diurnal maximum of precipitation in most numerical models (both global and regional) closely follows the diurnal maximum of surface sensible heating, indicating the dominance of parameterized convection (Basu 2007; Sen Roy et al. 2015; Davis et al. 2006) with overestimated precipitation frequency and underestimated precipitation

Responsible Editor: M. Telisman Prtenjak.

✉ Subhendu Brata Saha
sbsimd@gmail.com

[1] India Meteorological Department, New Delhi, India

[2] Department of Mathematics, Jadavpur University, Kolkata, West Bengal, India

intensity (Lin et al. 2000; Dai et al. 1999; Yang and Slingo 2001). Another major stumbling block in modelling tropical convection into numerical models is the wide spatial and inter-seasonal variations of convection over the continental regions. For example, studies have noted that the diurnal cycle of rainfall is stronger during the "break" period of the Monsoon over the Indian subcontinent as compared to the "active" period (Bhattacharya et al. 2017; Shige et al. 2017). A major stumbling block for estimating the character of moist convection using precipitation data in the tropics is due to the lack of a higher spatial and temporal scale surface-based observation network over of a large area, which is necessary to adequately measure the wide spatial scale of tropical convection, its nature and evolution of its diurnal characteristics.

Observing cloud processes from remotely sensed data has long been a standard approach in understanding the nature of moist convection. With the arrival of the Tropical Rainfall Measuring Mission (TRMM) and CloudSat satellites whose microwave channels penetrate through cloud layers, clouds are further separated into two types: convective and stratiform clouds. The separation has a physical basis. Observations indicate that the vertical profile of atmospheric heating is different in the convective and stratiform regions (Yuter and Houze 1995). Yang and Smith (2008), from a global 8 years dataset of TRMM precipitation radar (PR) and TRMM microwave imager (TMI) measurements, noted that across seasons, over continents, convective and total rainfall exhibit a consistent dominant afternoon peak. Stratiform rainfall over continents exhibits a consistent strong late evening peak and a weak afternoon peak, with the afternoon mode undergoing seasonal variability. They further suggest that diurnal modes largely arise from distinct diurnal stratiform variations modulating convective variations. Houze (1997) noted that stratiform and convective precipitations both occur within the same complex of convection-generated cumulonimbus cloud in the tropics; wherein the stratiform part of the cloud is associated with older precipitation while the younger portions of the cloud complex are primarily convective. Maddox (1980) defined mesoscale convective systems (MCS) from satellite-based cloud measurements, as a cloud system that occurs in connection with an ensemble of thunderstorms and produces a contiguous precipitation area on the order of 100 km or more in horizontal scale in at least one direction. Nesbitt and Zipser (2003) noted that over land areas, non-MCS features, enhanced by afternoon heating, have a significant peak in afternoon rain rates and intensity of convection, while MCS rainfall peaks occur in the late evening through midnight due to their longer life cycle.

The above studies provide a theoretical model for land convection in the tropics, i.e., convection (composed of growing cumulonimbus clouds) is maximum in the afternoon, in phase or slightly delayed with respect to the diurnal maximum of temperature. These then continue to grow into large systems of clouds, with gradually increasing areas of old convection and decreasing areas of fresh convection (leading to the increasing fraction of stratiform clouds compared to convective clouds in the total cloud cover). Convection again peaks in the late night–early morning hours, beyond when convection gradually decays down. In addition to the role of the diurnal cycle of temperature, this model of tropical convection also has an implicit role of humidity, which determines the lifetime of the convective systems after the afternoon peak is attained and allows for dissipation or maturation of convection into MCS stage and an early morning peak. While this model of tropical convection may generally be held true, local features modulate the type of convection and its maxima to a large extent creating large regional variations. This is especially true for weather episodes, when the atmospheric moisture content is not very high—as over Delhi. The role of the Himalayas in the night time growth of MCS and an early morning maximum along the Himalayan foothills has also been stressed in various studies (Romatschke and Houze 2011a, b). Studies indicate that over the plains of the Indian subcontinent, maximum convection preferentially occurred during the afternoon hours over the continental Indian subcontinent during the summer season (Yang and Slingo 2001; Basu 2007); although it gradually shifts to later hours as one moves northwestwards across the subcontinent (Sen Roy and Sen Roy 2014). Hence, in the triggering and development of convection over a region, the role of synoptic systems, coastal boundaries and mesoscale factors such as orography need to be investigated to create a more dynamic global model of the diurnal cycle of tropical convection and its spatial and seasonal variations. This requirement for detailed analysis of the three-dimensional features of convective weather and their evolution on a diurnal scale during an event is only possible from high-resolution, three-dimensional, continuous data, which is available from weather radars. This study looks in detail at the diurnal cycle of convection over northwest India for multi-day rainfall events which have resulted from three different kinds of synoptic systems over the region, utilizing the weather radar data from a Doppler radar installed at Delhi as well as data of the atmosphere at the time of convection. The purpose is to delineate the common features of the diurnal variability of convection over this inland station and investigate the role of various triggering factors in changing the character of convection for different kinds of weather systems. The results are representative of multiple other cases, which have been analyzed across seasons. The weather radar network of India, its data and configuration are detailed elsewhere (Roy Bhowmik et al. 2011).

In Sect. 2, we discuss the climate of Delhi and the motivation for selecting the cases for detailed study. In Sect. 3,

we discuss the data and methodology of analysis. Section 4 explain the observed results while in Sect. 5, these results have been summarized and conclusions made.

2 Climate of Delhi

Delhi is located on the northern part of the Indian subcontinent (Fig. 1). As per Köppen classification, this region is classified as sub-tropical semi-arid climate and is generally dry, except the monsoon season during July to September (Peel et al. 2007). Moisture inflow from the surrounding Arabian Sea and Bay of Bengal causes rainfall episodes (Sen Roy and Sen Roy 2011). During the non-monsoon period (October–June), extra-tropical westerly troughs in the mid troposphere pass over the region. The low-pressure zone ahead of the trough, over North India, pulls in moisture from the surrounding seas (Arabian Sea and the Bay of Bengal), thereby moistening the atmosphere and creating short-lived rainfall episodes. Less frequently, large tropical cyclones in the surrounding seas pump moisture deep inland up to northern part of India and cause rainfall episodes. During monsoon season (July–September), the atmosphere is generally more moist. Monsoon low-pressure systems and depressions originate in the Bay of Bengal, and move northwestwards across the Indian subcontinent along the monsoon trough and bring long-lived rainfall episodes associated with deeper moisture flow from the Arabian Sea and Bay of Bengal into this region (Rao and Srinivasan 1968; Sen Roy and Sen Roy 2011, 2014).

Radar analysis of the Delhi region, using hourly data from the Japanese radar (NMD-45), through 1000–1700 h Indian Standard Time (IST) for 100 km around Delhi, during the period 1958–1980 have documented that the cumulonimbus cloud with tops exceeding 12 km is minimum during winter and maximum during monsoon season (Chatterjee and Prakash 1986). This study also noted that the cloud top height exceeding 16 km (tropopause level over Delhi) is observed during the months from May to October. In terms of associated weather, synoptic observations note that over Delhi region, squally winds associated with thunderstorms are most severe during the pre-monsoon season (March–May) (Ram and Mohapatra 2012), while their peak frequency of occurrence is observed between 1500 and 2100 h IST (Bhalotra 1954).

Figure 2a displays the climatological vertical profile of the wind field over Delhi [India Meteorological department (IMD) Radiosonde/Radiowind normal for the period 1971–1990]. Two soundings are taken daily at 00 UTC (0530 IST) and 12 UTC (1730 IST). The average vertical profile from both soundings—two for each month—is plotted alternately in the same vertical time section. As may

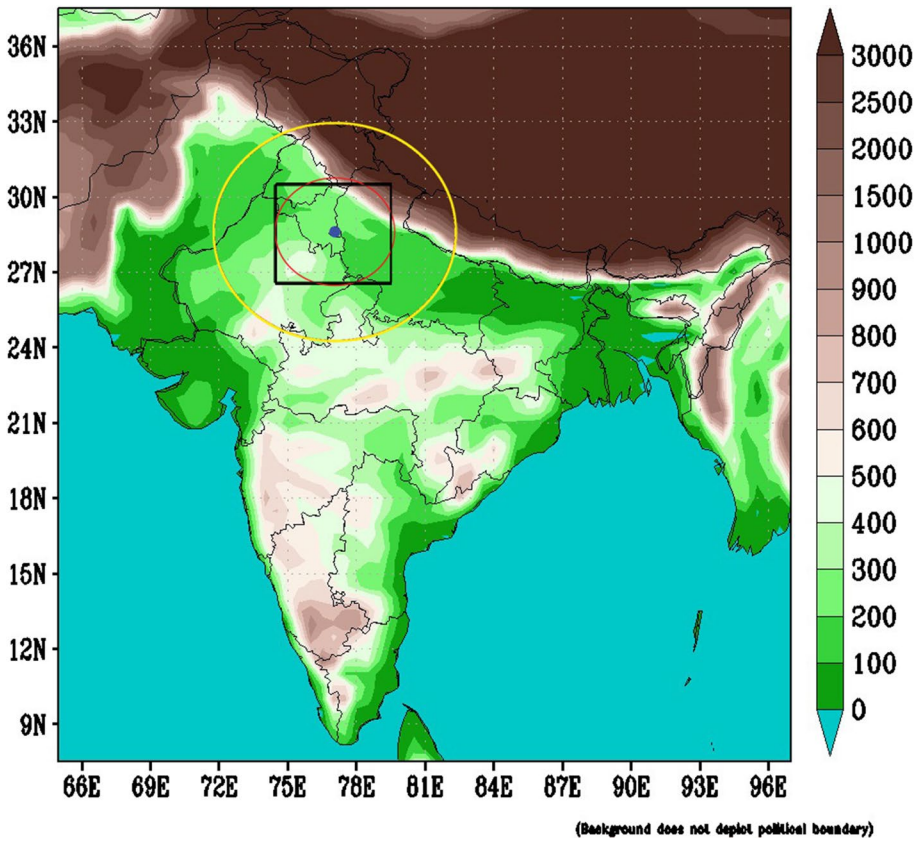

Fig. 1 Location of Delhi and surrounding states on a terrain map (in m) of the Indian subcontinent. The inner box delineates the domain of study around the Delhi radar. The yellow circle denotes the domain of radar view (500 km), while the red circle denotes the radar coverage of 250 km used for detailed analysis

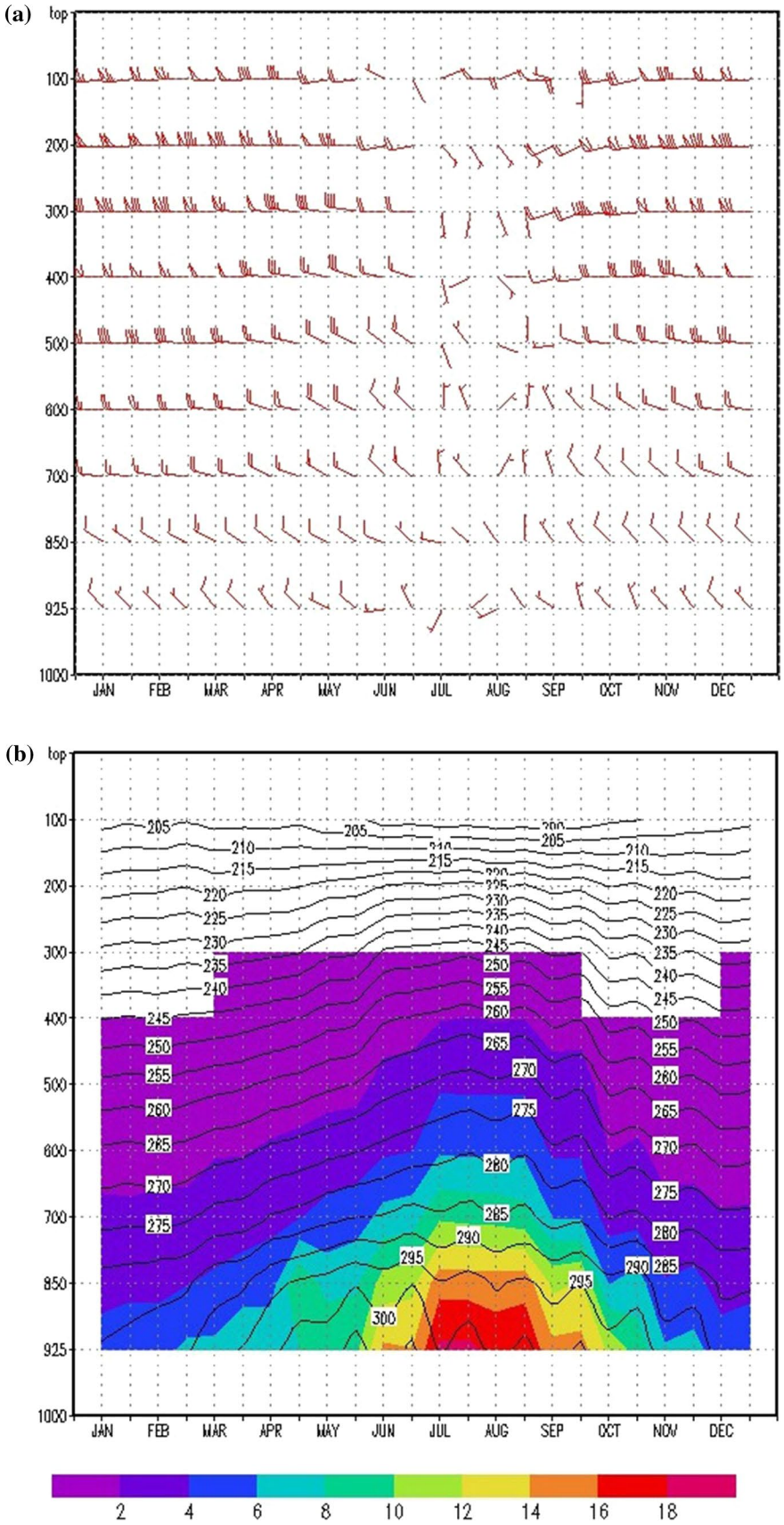

Fig. 2 Monthly climatological vertical profile of the **a** wind field (in knots), **b** temperature (black contours in K), superposed by specific humidity (filled contours in g/kg) field over Delhi. For each month, two sets of observations at 0530 IST and 1730 IST are plotted in the same figure (1971–1990 IMD Radiosonde/Radiowind NORMALS)

be seen, the wind profile is calmest during July–September and winds are strongest during December to March when the total atmospheric shear is also maximum. This is because, for most of the year (non-monsoon period, i.e., October–May), Delhi is located in a westerly regime where the wind field strengthens with height to the Sub Tropical Westerly Jet (STWJ). The STWJ is in its most southward location, lowest position in the troposphere and most intense during winter season—November to March (Schiemann et al. 2009)—which corresponds to the Delhi latitude, resulting in the high vertical shear in the atmosphere. During the monsoon period, northward movement of the continental Inter tropical Convergence zone over the Asian land mass causes weak easterlies to penetrate into the Indian subcontinent and North India becomes a region of low wind speeds. Figure 2b displays the climatological vertical profile of the temperature (black contours), super-imposed by the vertical profile of the specific humidity (filled contours). In this case too, the average vertical profile from both soundings—two for each month—is plotted alternately in the same vertical time section. It may be noted that the lower tropospheric temperature is highest during early summer (May and June) which does not coincide with the period when moisture is maximum (July–September). Consequently, three distinctly different cloud regimes emerge over the region as noted by Sen Roy et al. (2014), which can be defined in relative terms. They are:

(a) an environment of relatively high shear (500 hPa and below) and low diabatic heating in winter and pre-monsoon (December–April), when short-lived mesoscale cloud structures under a thick cold upper level stratiform (cirrus) cover develops, producing short episodes of rain, during the passage of deep westerly troughs [also observed by Puranik and Karekar (2009)],
(b) an environment of relatively moderate shear, high sensible heating and low latent heating (May and June), when short-lived, tall, fast-moving narrow cells with high reflectivity develops in the afternoon hours and are sometimes organized into short-lived squall lines. Low-level vertical shear (below 700 hPa) is highest during this period, which is favourable for occasional formation of squall lines (Weisman and Klemp 1982),
(c) an environment of relatively low shear, moderate sensible heating and high latent heating (July–September), when broad cells with moderately high reflectivity and long lifetimes develop in slow-moving convective zones.

For the purposes of this study, we define a convection region or zone as a horizontal region of contiguous reflectivity values detected by a radar, with reflectivity values greater than 5 dBZ [similar to the definition of Houze et al. (1989)]. We define life span of an episode as the length of time when there is intermittent presence of convection regions and rainfall in the domain of the radar during the entire period. These regions comprise of cells in different stages of development as well as the stratiform remnants from old cells. Multiple convection regions with different life spans and characteristics may arise concurrently in different parts of the radar domain throughout the period of influence of a synoptic system over that region while their organization is dependent upon the nature of the synoptic system as well as the vertical structure of the atmosphere over the station. While the lifetime of individual cells in these convection regions vary from 10 to 30 min, life span of a convection region ranges from an hour (for winter and early pre-monsoon weather systems) to days (during monsoon weather systems) making them easier to monitor. To analyze the diurnal evolution of the characteristics of these convection regions during a weather episode, it is necessary to consider continuous measurements of long-lived episodes from ground-based weather radars with a sub-hourly sampling rate. This accent on the diurnal aspects of evolution of the convection regions eliminates winter and early pre-monsoon systems, when the episodes are sub-daily.

Figure 3 illustrates the daily average rain rate (mm per day) over the domain surrounding Delhi during 2014 as obtained from the TMPA (TRMM 3B42) products. Figure 4 represents the values of precipitable water content of the atmosphere and vertical shear (calculated over a 6 km depth from the surface) from the radiosonde profile on these days during rainy day of April to September. The figure indicates month wise clustering of rain events indicating systematic shift in weather conditions during rainfall episodes over the course of the year. As discussed before, for rainfall events during July, August and September, the precipitable water content is high and shear values are low. Precipitable water content is low for rainfall events during April, May and June. Shear values are generally high during April and more variable during May and June. Out of the entire gamut of weather conditions during rainfall episodes throughout the year, three representative cases have been selected for detailed analyses. They are (a) a pre-monsoon season rainfall episode of May 30–31, 2014 in association with the movement of a mid-tropospheric westerly upper air trough over the region; (b) a late pre-monsoon episode of June 12–13 2014 associated with moisture feeding into the region from a tropical cyclone in the Arabian Sea; and (c) a rainfall episode during summer monsoon season in association with the movement of low-pressure systems to over the region, from the Bay of Bengal during September 3–5, 2014. Case 1 represents low precipitable water, moderate shear environmental conditions, case 2 represents higher shear, but similar precipitable water conditions,

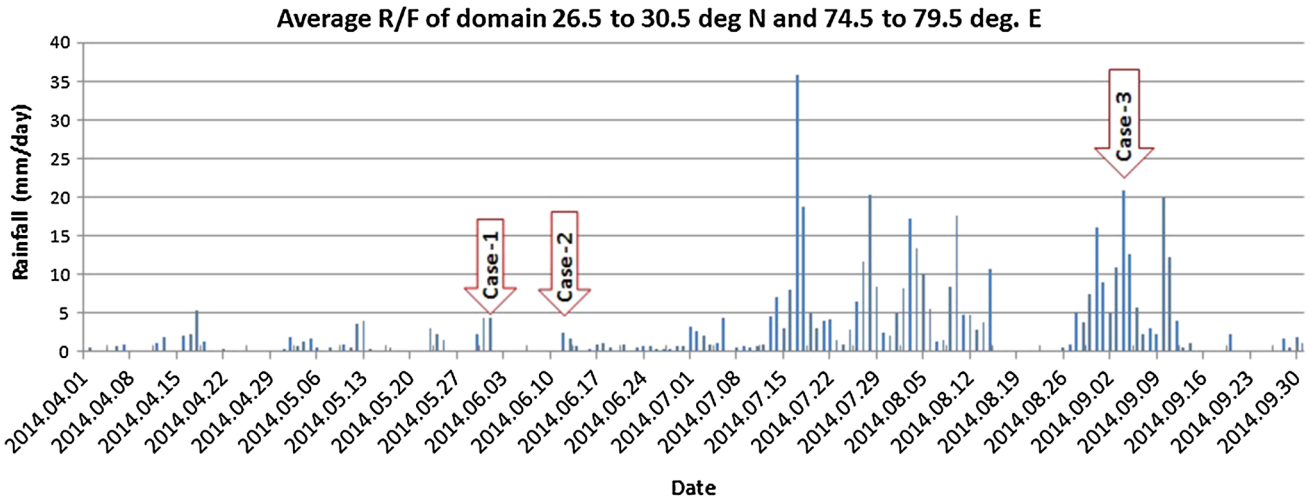

Fig. 3 Average daily rain rate (mm/day) as per TRMM 3B42 dataset through 2014, averaged over the entire domain (Lat 26.5–30.5°N and Lon 74.5–79.5°E) under consideration. Arrow indicating the day for case 1 (May 30–31), case 2 (June 12–13) and case 3 (September 3–5)

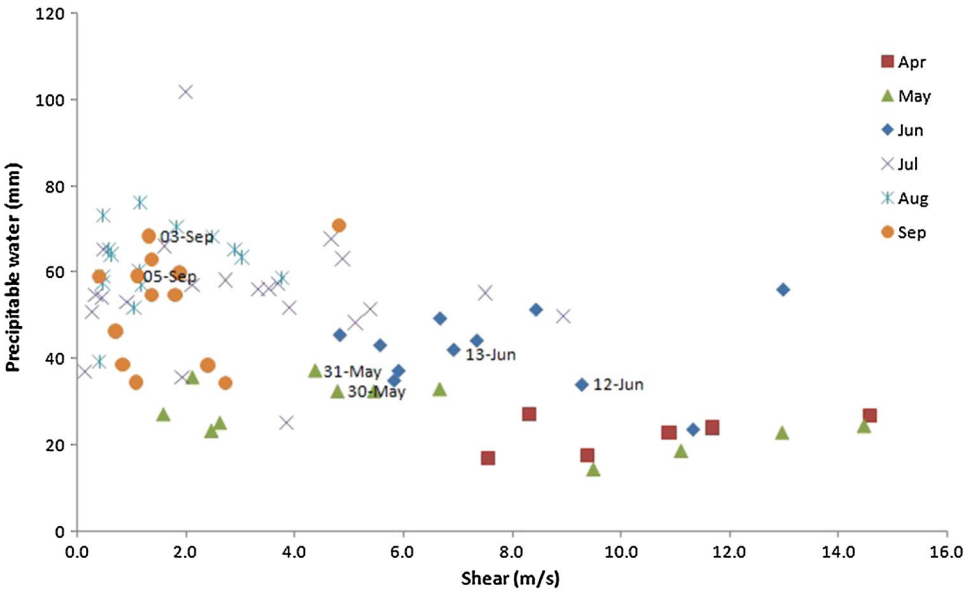

Fig. 4 Precipitable water (pptw) content of the atmosphere versus vertical shear (calculated over a 6 km depth from the surface) from the radiosonde profile over Delhi during rainy day of April to September 2014. The *x*-axis denotes the vertical shear (in m/s) and *y*-axis is corresponding pptw (in mm). Colour legend of data points indicate each month from April to September

while case 3 represents high precipitable water, low shear environmental conditions. The features of the weather systems, discussed hereafter, were found to be representative of other weather systems over the region occurring in similar environmental conditions. These specific episodes were selected for detailed analysis, based on the following criteria: (a) availability of continuous radar data for 48 h or more, during the episode. (b) Cloud system should pass within 250 km of location of the radar for most of the lifetime of the systems, so that it is possible to clearly delineate the cloud structure from the radar reflectivity profiles.

3 Datasets and methodology

The C-band radar, whose data is used in the present case, is located at Delhi and it scans the surrounding volume, once every 10 min. It follows a hybrid scan strategy, covering up to 500 km for reflectivity in the lower elevations (up to 2° elevation angle) and 250 km in the higher elevations (up to 21° elevation angle) [for details please see Roy Bhowmik et al. (2011)]. However, since the structure of the cells is less defined further away from the radar, we have limited the Cartesian analysis to a 250 km range around the radar.

The radar reflectivity data are used to construct Hövmoller diagrams (altitude versus time) of the normalized hourly reflectivity count field for each rainfall episode, by the following method.

The radar measurements, which are available in spherical coordinates (range, azimuth, and elevation), are interpolated to regularly spaced longitude–latitude grids, in constant height surfaces using the package "Radx" (assembling SPRINT and CEDRIC) developed by L. Jay Miller and Mike Dixon at NCAR RAL (USA) for a more rigorous analysis of the radar reflectivity data. The package is available as a part of the TITAN package on their site. The software uses the legacy SPRINT (Sorted Position Radar INTerpolator) software algorithms developed by Mohr and Vaughan (1979) and Mohr et al. (1981) to convert the radial data to Cartesian coordinates. The major steps involved in the processing are (a) interpolation of data to Cartesian grid (b) removal of noisy data, (c) filling data voids, and (d) data filtering. The software uses a three-dimensional linear interpolation scheme to populate the output grid comprising of 20 levels at 1 km height intervals starting from 1 km a.m.s.l. for a 250 km range around the radar. Interpolation is done in a piece-wise continuous, bilinear method with local unfolding of radial velocities and reflectivity. This scheme optimally uses eight radar measurements (two bins along a ray, from two adjacent rays in the azimuthal direction, and two adjacent elevations) that surround the output grid point. In the present case, the IMD NETCDF format data are first converted to CFRADIAL compliant NETCDF data file. These files are input to the "Radx" package for interpolating radial data to a regularly spaced longitude–latitude grid, at constant height surfaces. The final Cartesian grid is a 500–500 km box in the horizontal with 0.5 km x–y resolution and 20 km height in the vertical with 1 km resolution. Assuming that the radar volume will change appreciably only every 20 min, three 3-D Cartesian coordinate regularly spaced gridded reflectivity volume files are computed at 20-min intervals for each hour. The reflectivity pixels from the three files are then summed over at each level, as well as spatially at each level, for values greater than a given threshold. This reflectivity pixel count at each level is then divided by the total grid points of the domain of study and multiplied by 100 to get the normalized reflectivity count for individual vertical level. These hourly one-dimensional profiles (height versus normalized reflectivity counts) are then plotted in time during an entire rainfall episode, to observe the evolution of the reflectivity profile of the cloud population over the domain. The analysis is similar to the contoured frequency by altitude diagrams by various previous studies [Houze et al. (2007) for example]. However, unlike the previous studies, the present plot additionally shows the temporal evolution of the profiles. Two reflectivity thresholds of 20 dBZ and 40 dBZ were selected for detailed analysis. The lower threshold can be roughly associated with rainfall rates of 0.5 mm/h (Marshall and Palmer 1948). Although this relationship is not so straightforward, it would be reasonable to assume that the 20-dBZ isopleth delineates the precipitating clouds (Laurent et al. 2002). On the other hand, various studies have noted the 40 dBZ threshold correspond to convective type of precipitation (Tokay and Short 1996; Churchill Dean and Houze 1984; Steiner et al. 1995; Romatschke et al. 2010). This does not imply that the cloud pixels with reflectivity below 40 dBZ automatically correspond to stratiform clouds, except where bright band is present; rather a mixed cloud cover is expected below 40 dBZ, while pixels above 40 dBZ denote a primarily convective cloud regime unless present at the freezing level. In addition, only the vertical profile above 4 km height and up to 20 km is considered for analysis. This is because, according to the range, height and elevation angle relationship with the curvature of the earth, even at the lowest angle, the beam tilts away from the earth at greater range values. Hence, while reflectivity values at lower heights are available closer to the radar, this is not so, further away. The lowest height for which, uniform values are available for the entire domain is at 4 km height above the radar. In addition, by considering the bottom threshold $\geq$4 km, terrain-related partial beam blockage at low elevation angles over Delhi by the surrounding Aravalli hills is also accounted for (Serafin and Wilson 2000; Maddox et al. 2002). Hence we get two such plots per rainfall episode corresponding to the two different thresholds. The altitude–time plots for 20 and 40 dBZ thresholds for three different cases are plotted in Figs. 5a, b, 6a, b, and 7a, b.

The corresponding 3-hourly rain rate values over the domain are obtained from the TMPA (TRMM Multisatellite Precipitation Analysis) 3B42 dataset (Huffman et al. 2007). This is a spatially uniform measure of rainfall and has been observed to give good results over the Indian plain region (Rahman et al. 2009; Nair et al. 2009). The total rain rate per hour within the analysis box from the TMPA 3B42 Version 7 dataset at 0.25° grid resolution is averaged for the entire domain to obtain the rainfall pattern of the preceding 3 h. This is plotted in Fig. 8a–c for the three cases, respectively.

The National Centre for Environmental Prediction (NCEP) Global Forecast System (T-574) model analysis fields, initialized at 00 UTC every day, run at IMD, New Delhi [details of the model configuration may be seen in (Durai and Roy Bhowmik 2013)], are used to analyze the synoptic conditions associated with the weather systems. These are plotted for 300 hPa, 500 hPa, 850 hPa and 925 hPa for each case (Figs. 9a–d, 10a–d and 11a–d for the three cases, respectively).

The upper atmosphere wind and temperature vertical profile, used to analyze the diurnal variation of the atmosphere for various cases in this study, are from the twice daily (0530 and 1730 IST soundings) data of the Indian radiosondes as

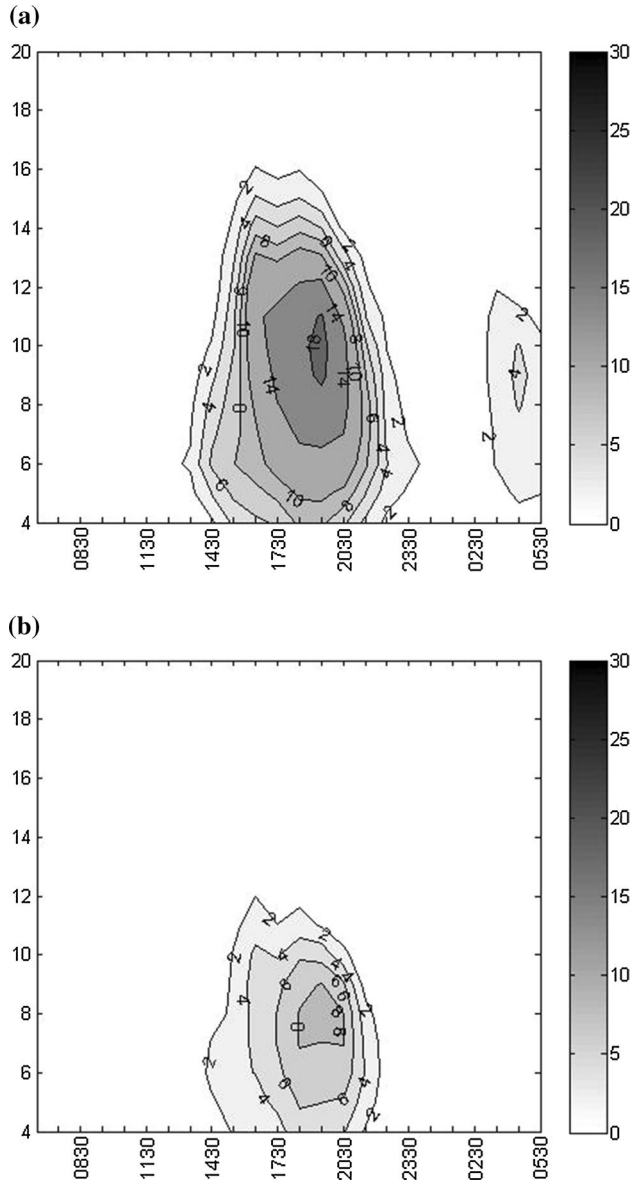

Fig. 5 Hövmoller diagrams for percentage value of pixel count of total pixel count over domain of study with a threshold dBZ value of **a** 20 dBZ and **b** 40 dBZ. *x*-axis values are IST time starting from 0630 IST of 30th to 0530 IST of 31st May 2014. *y*-axis values are height in km

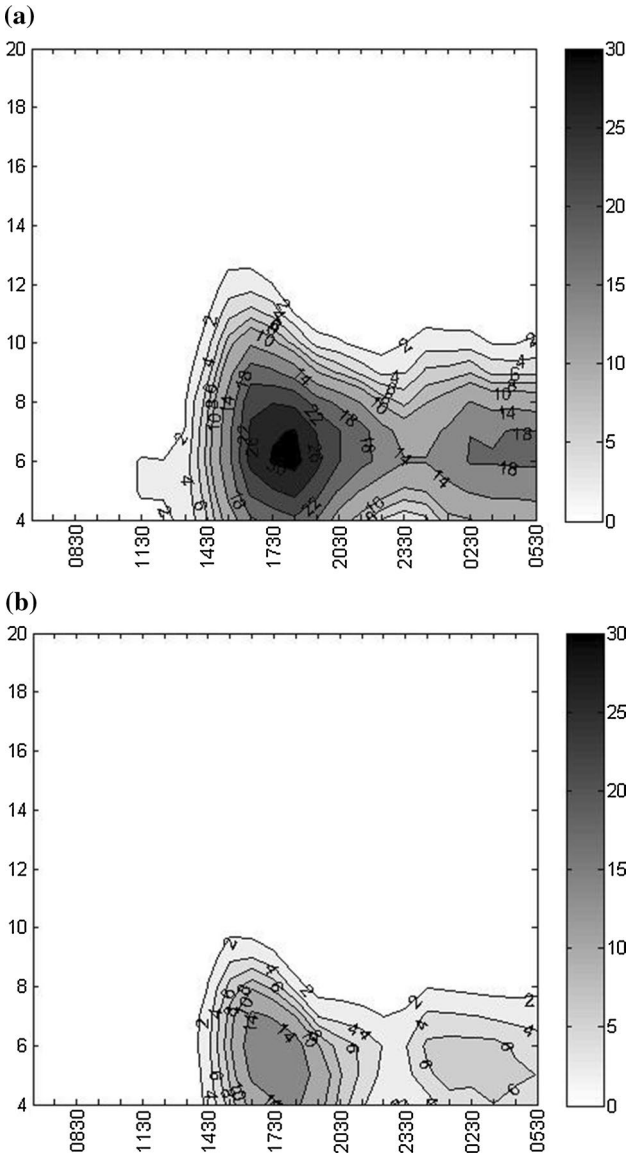

Fig. 6 Hövmoller diagrams for percentage value of pixel count of total pixel count over domain of study with a threshold dBZ value of **a** 20 dBZ and **b** 40 dBZ. *x*-axis values are IST time starting from 0630 IST of 12th to 0530 IST of 13th June 2014. *y*-axis values are height in km

collected from the website http://weather.uwyo.edu/upperair/sounding.html. The data of the two soundings everyday are plotted in the same vertical time section around each rainfall episode in Figs. 12a, b, 13a, b and 14a, b for the three cases, respectively.

The moisture data are discontinuously obtained from the radiosonde observations. Therefore, to analyze the diurnal cycle of moisture during the three episodes, the vertical profile of the specific humidity field from European Reanalysis (ERA)-Interim Reanalysis is used. ERA-Interim represents a third-generation global atmospheric reanalysis produced by the European Centre for Medium-Range Weather Forecasts (ECMWF). These data reanalyses permit in-depth analysis of the diurnal cycle of the atmosphere. Configuration and performance of the data assimilation system describing the ERA-Interim Reanalysis are available from Dee et al. (2011). Gridded data products include a large variety of 6-hourly upper-air parameters covering the troposphere and stratosphere. The time series of vertical profile for specific humidity at spatial resolution of $0.25° \times 0.25°$ are averaged over the domain of study and are plotted in Fig. 15a–c for the three cases in this study, respectively.

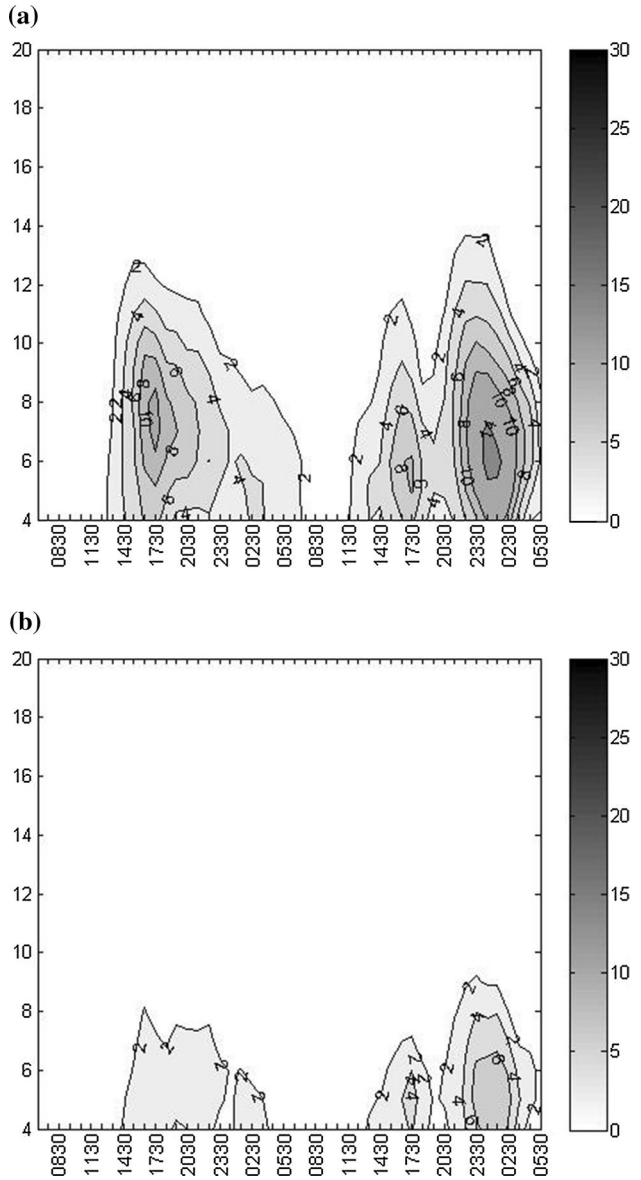

Fig. 7 Hövmoller diagrams for percentage value of pixel count of total pixel count over domain of study with a threshold dBZ value of **a** 20 dBZ and **b** 40 dBZ. *x*-axis values are IST time starting from 0630 IST of 03rd September to 0530 IST of 05th September 2014. *y*-axis values are height in km

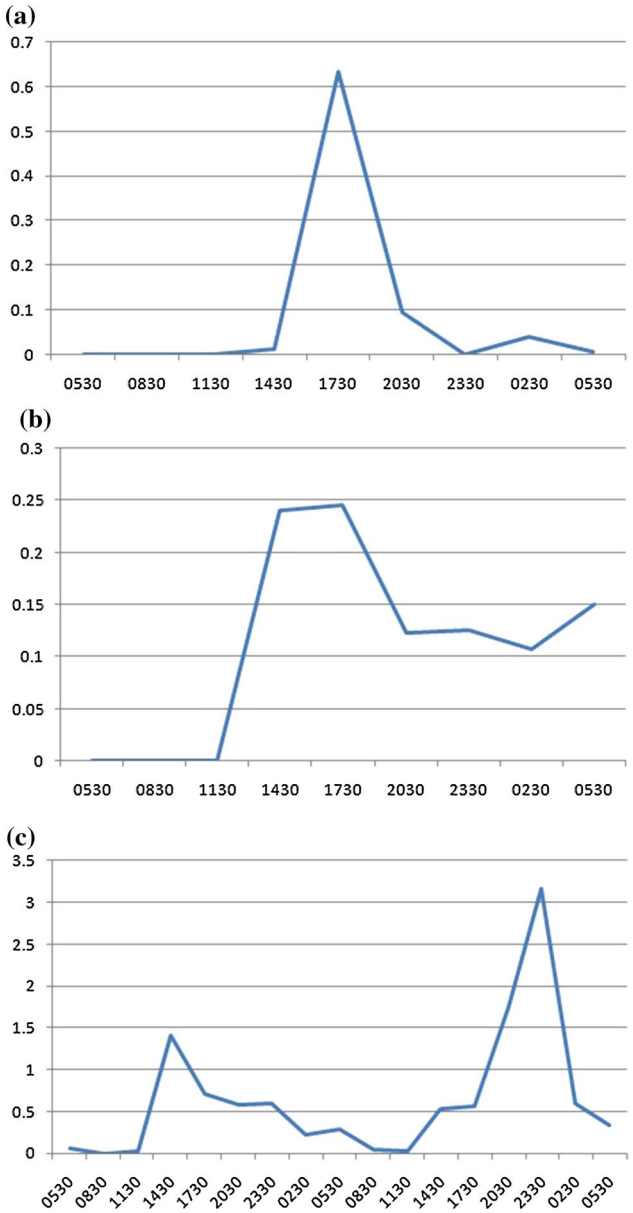

Fig. 8 TRMM 3B42 3-hourly average rain rate for the domain as estimated by the TRMM 3B42 dataset. *x*-axis values are IST time starting from **a** 0530 IST of 30th to 0530 IST of 31st May 2014, **b** 0530 IST of 12th to 0530 IST of 13th June 2014, and **c** 0530 IST of 03rd to 0530 IST of 05th September 2014. *y*-axis values are domain average rain rate (in mm/h)

4 Results

4.1 Case 1: (30–31 May 2014)

This was a pre-monsoon season rainfall episode over the Delhi region. A westerly trough moved over to the North Indian region during 29–31 May 2014 before moving away eastwards. Figure 9a–d displays the model analysis map fields of NCEP Global Forecast System (T574 at 22 km resolution) initialized at 0530 IST of 30th May 2014 for 300 hPa, 500 hPa, 850 hPa and 925 hPa, respectively.

As inferred from the above maps and Indian Daily Weather Report issued by IMD, in association with an upper level westerly trough at 500 hPa over North Pakistan and neighbourhood, an induced cyclonic circulation was formed, ahead of the trough in the lower troposphere in the neighbourhood of Delhi (at 850 hPa and below) during 29–31 May (as may be seen in Fig. 9c for 30th May 2014). This was embedded in an east–west trough also in the lower troposphere (925 hPa and below from 74°E to

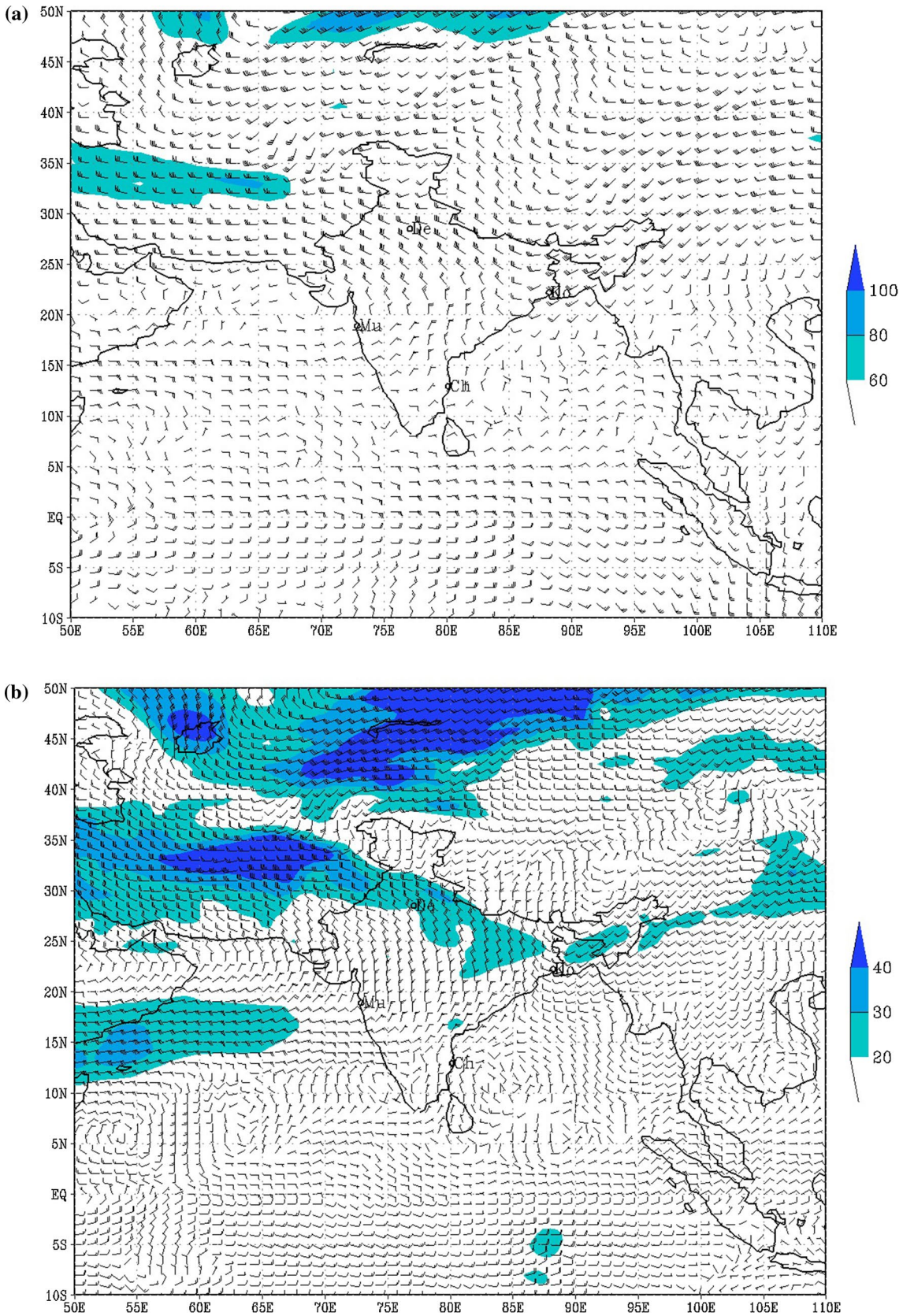

Fig. 9 GFS model runs at IMD initialized at 0530 IST of 30th May 2014. Analysis wind field of 0530 IST of 30th May 2014 at **a** 300 hPa level, **b** 500 hPa level, **c** 850 hPa level, and **d** 925 hPa level. Colour contours are for isotach as per colour bar (in knots). 'De' denotes the location of Delhi

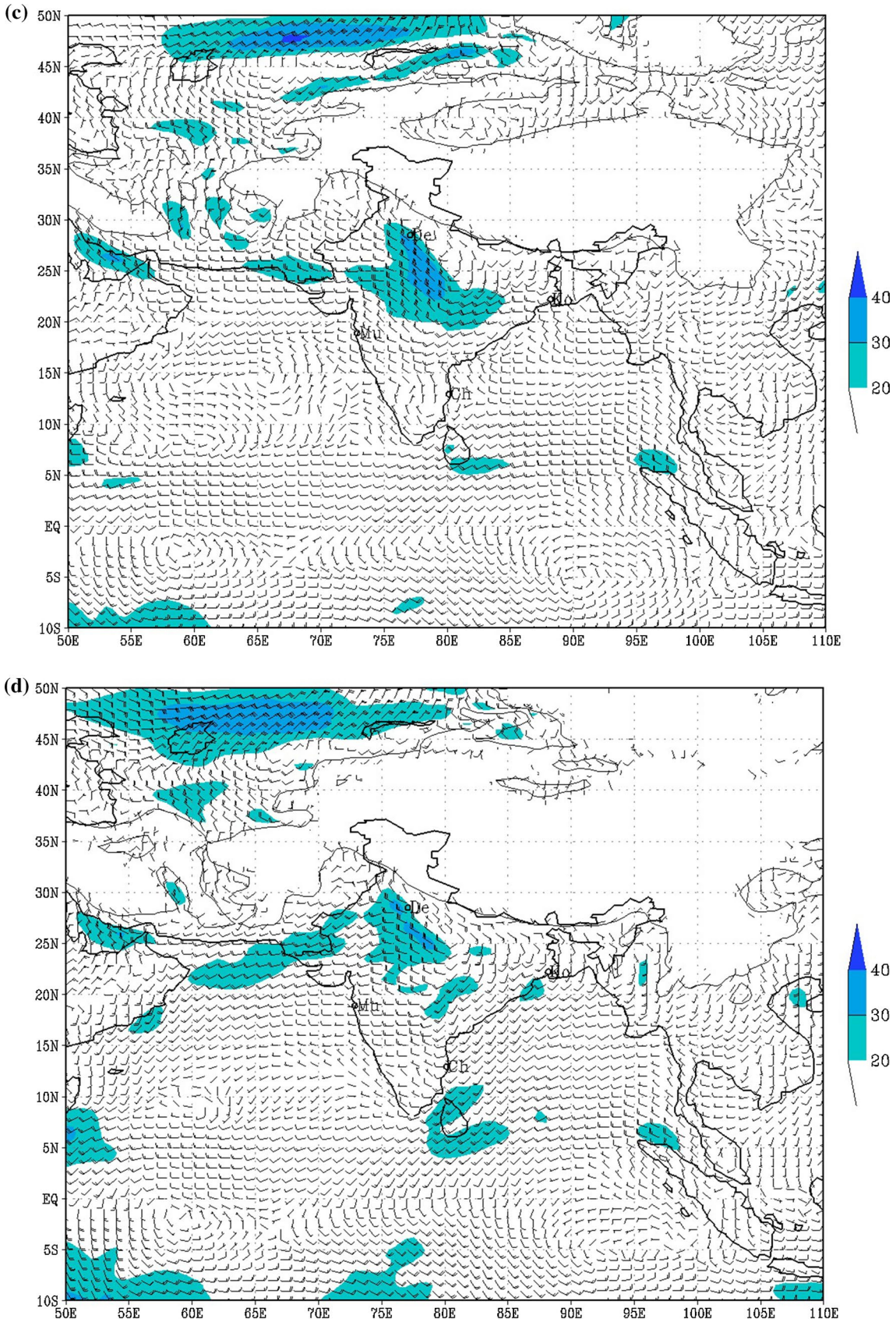

Fig. 9 (continued)

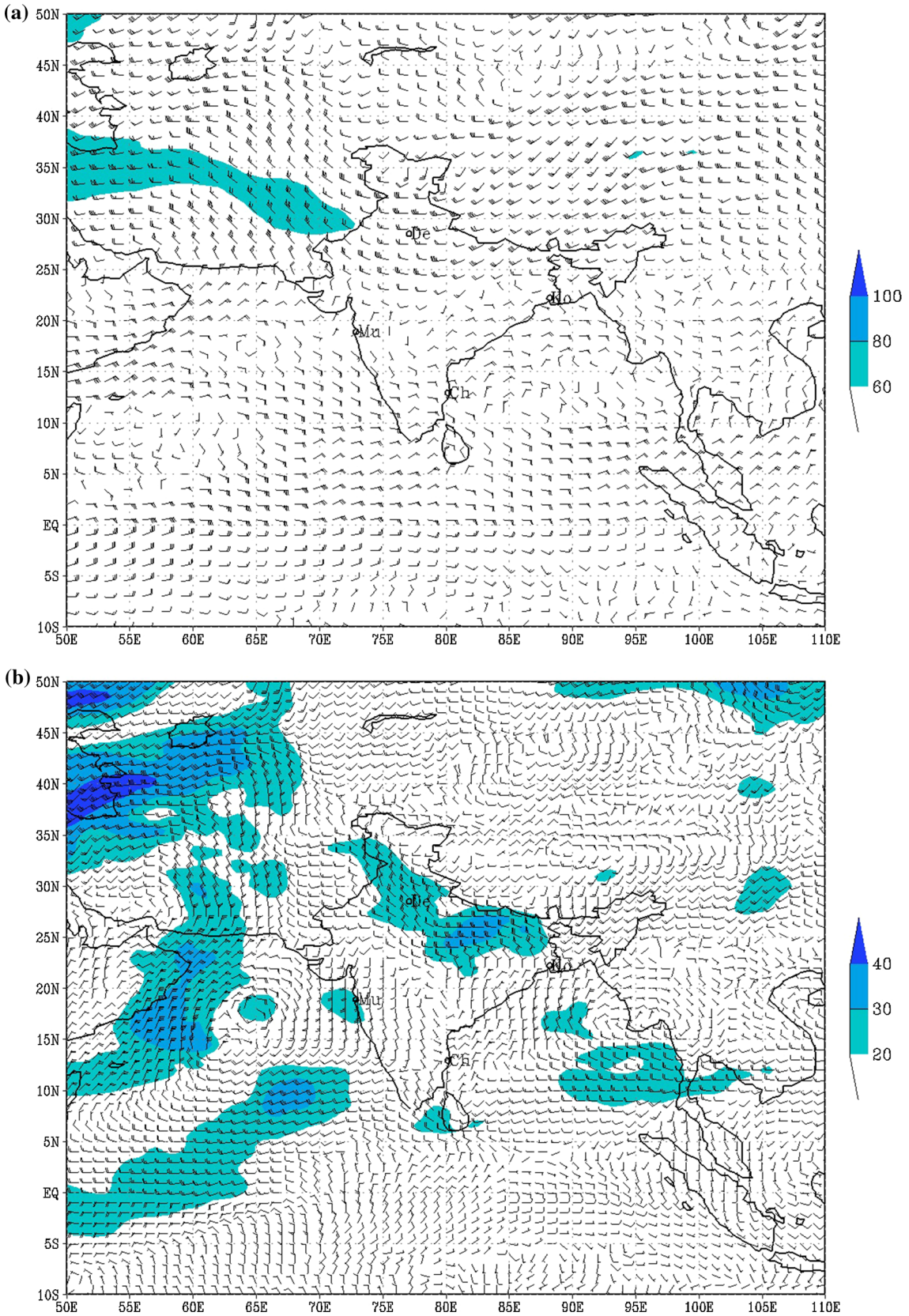

Fig. 10 GFS model runs at IMD initialized at 0530 IST of 12th June 2014. Analysis wind field of 0530 IST of 12th June 2014 at **a** 300 hPa level, **b** 500 hPa level, **c** 850 hPa level and **d** 925 hPa level. Colour contours are for isotach as per colour bar (in knots). 'De' denotes the location of Delhi

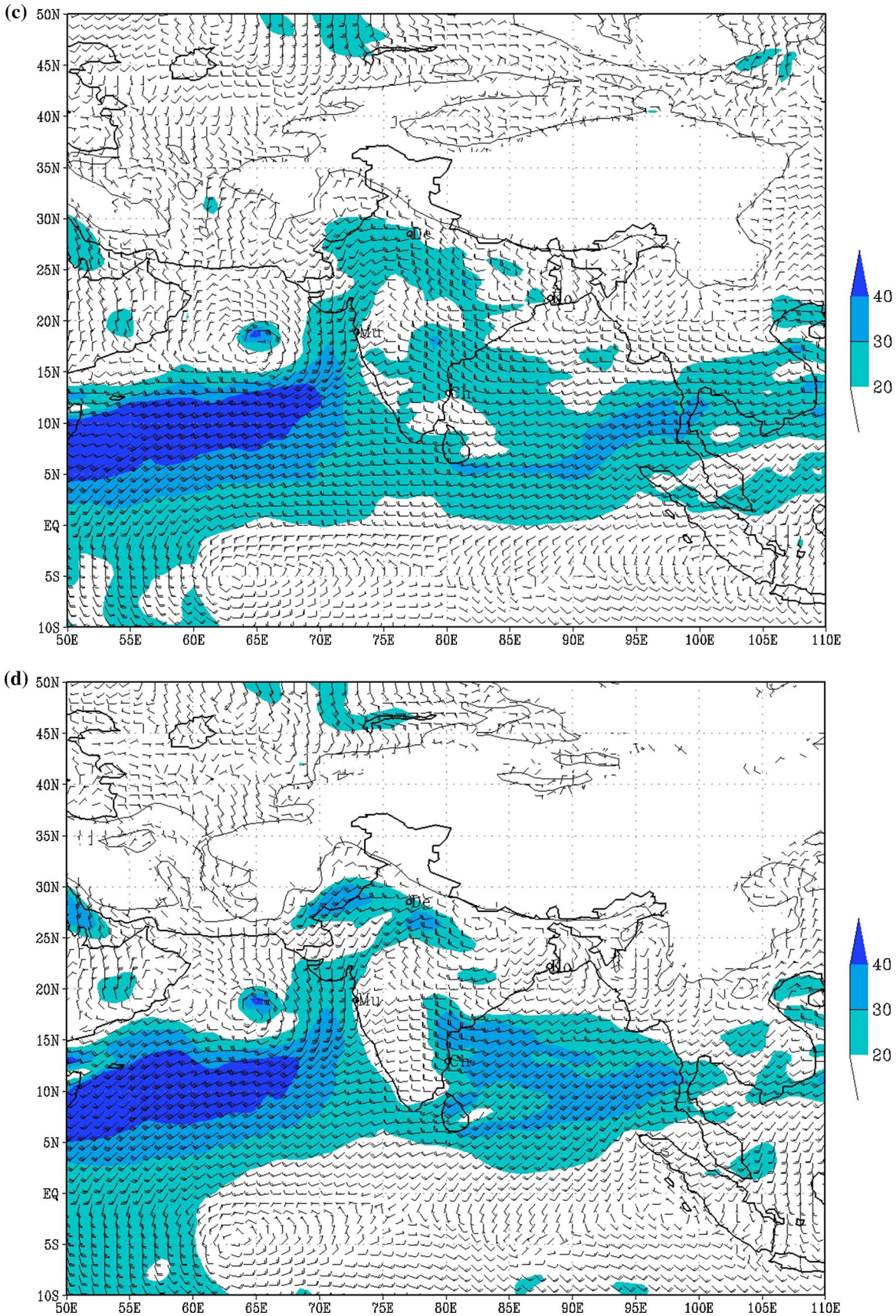

Fig. 10 (continued)

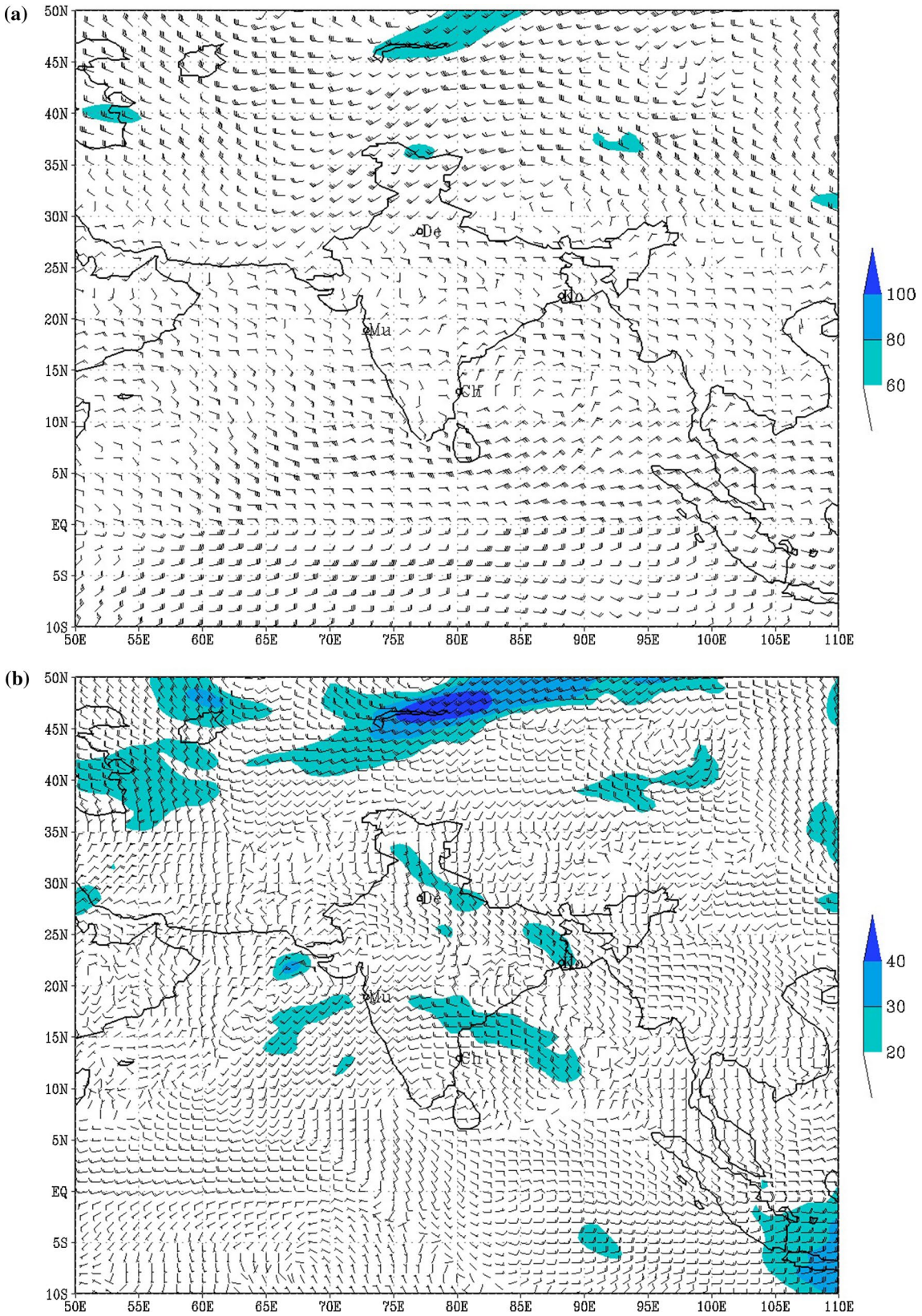

Fig. 11 GFS model runs at IMD initialized at 0530 IST of 03rd September 2014. Analysis wind field of 0530 IST of 03rd September 2014 at **a** 300 hPa level, **b** 500 hPa level, **c** 850 hPa level and **d** 925 hPa level. Colour contours are for isotach as per colour bar (in knots). 'De' denotes the location of Delhi

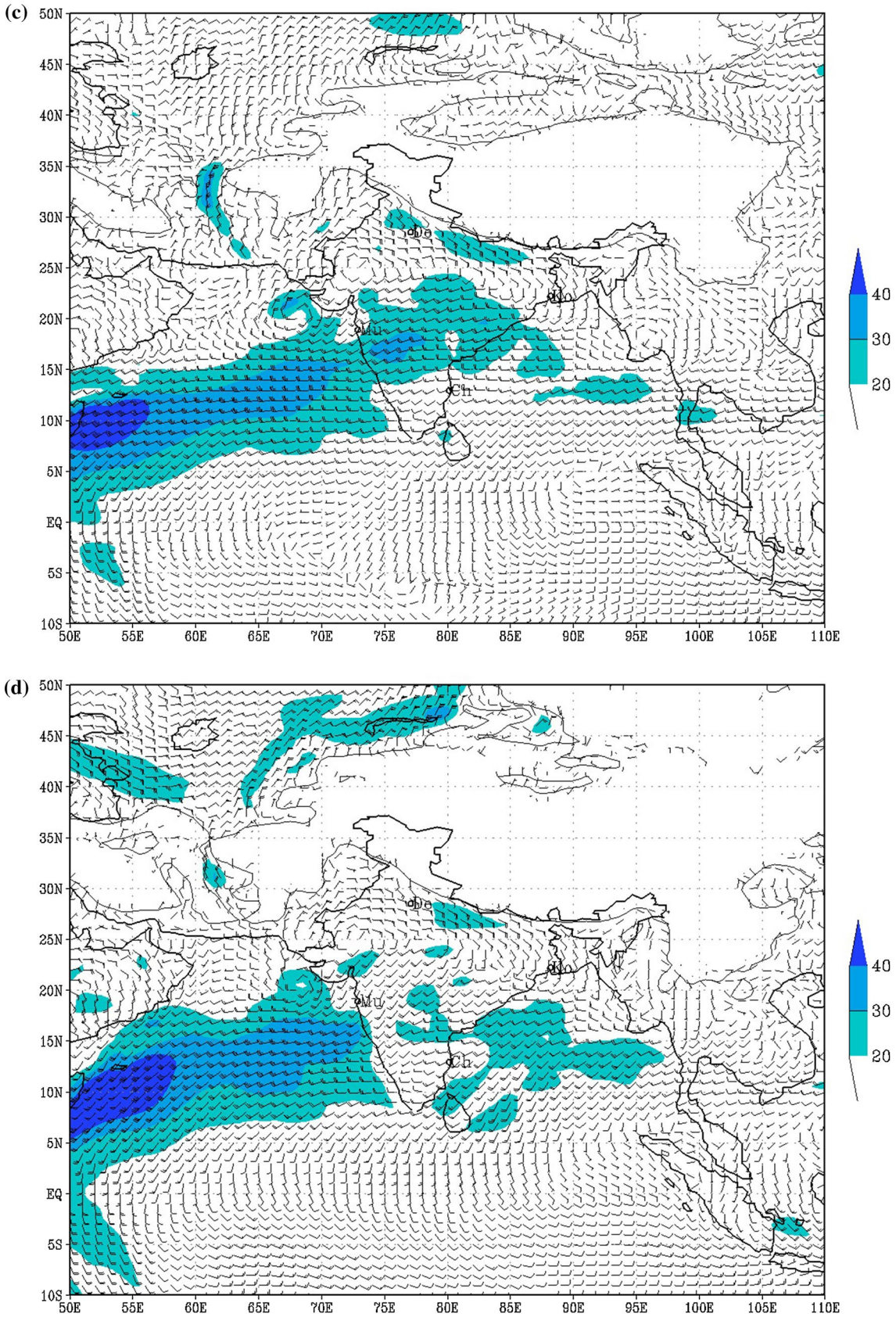

Fig. 11 (continued)

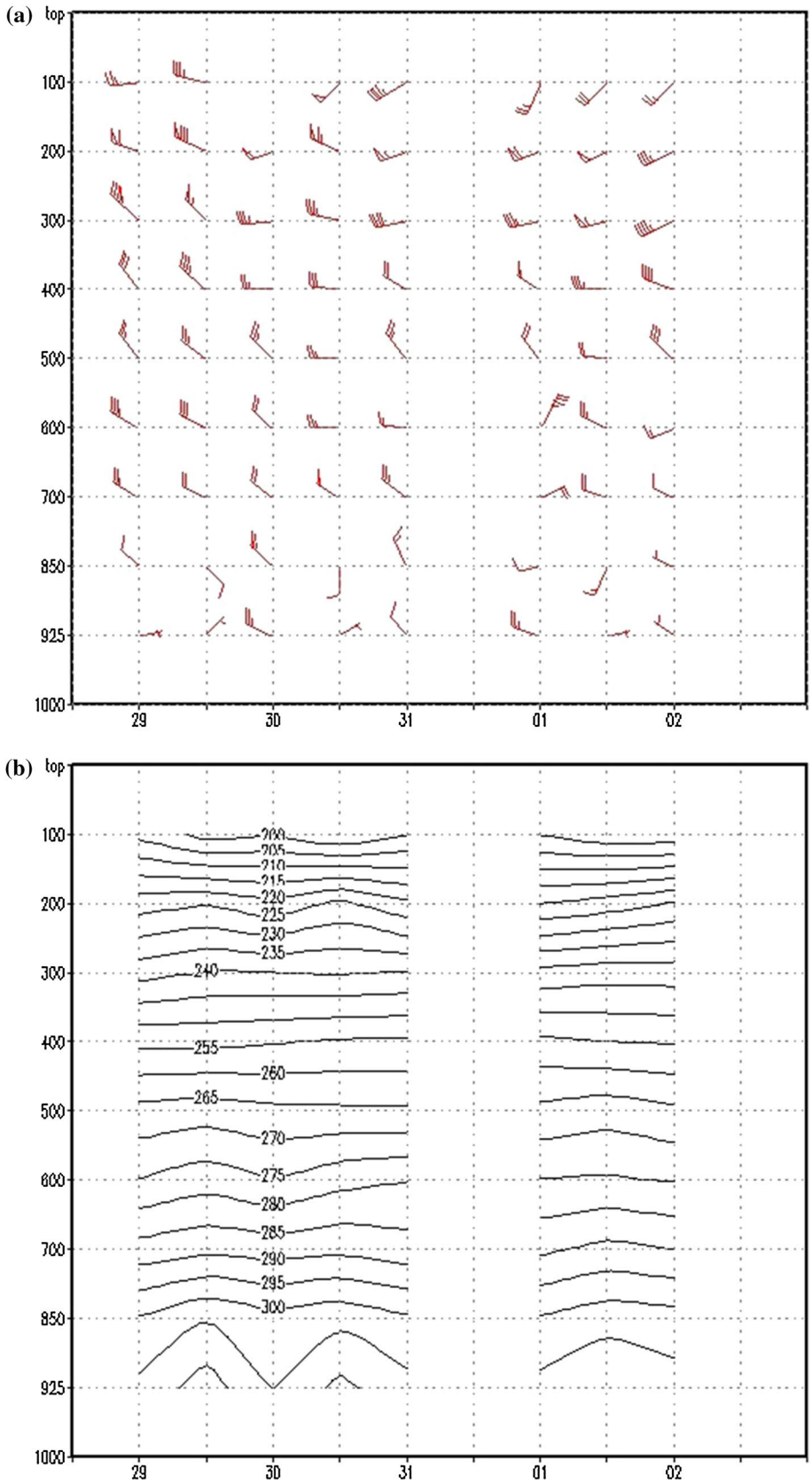

Fig. 12 Vertical profile of the **a** wind field (in knots) and **b** temperature field (K in black contours), over Delhi during the period 29th May to 02nd June 2014. For each day, two sets of observations at 0530 IST and 1730 IST are plotted in the same figure. *x*-axis denotes the date and *y*-axis is pressure levels in hPa

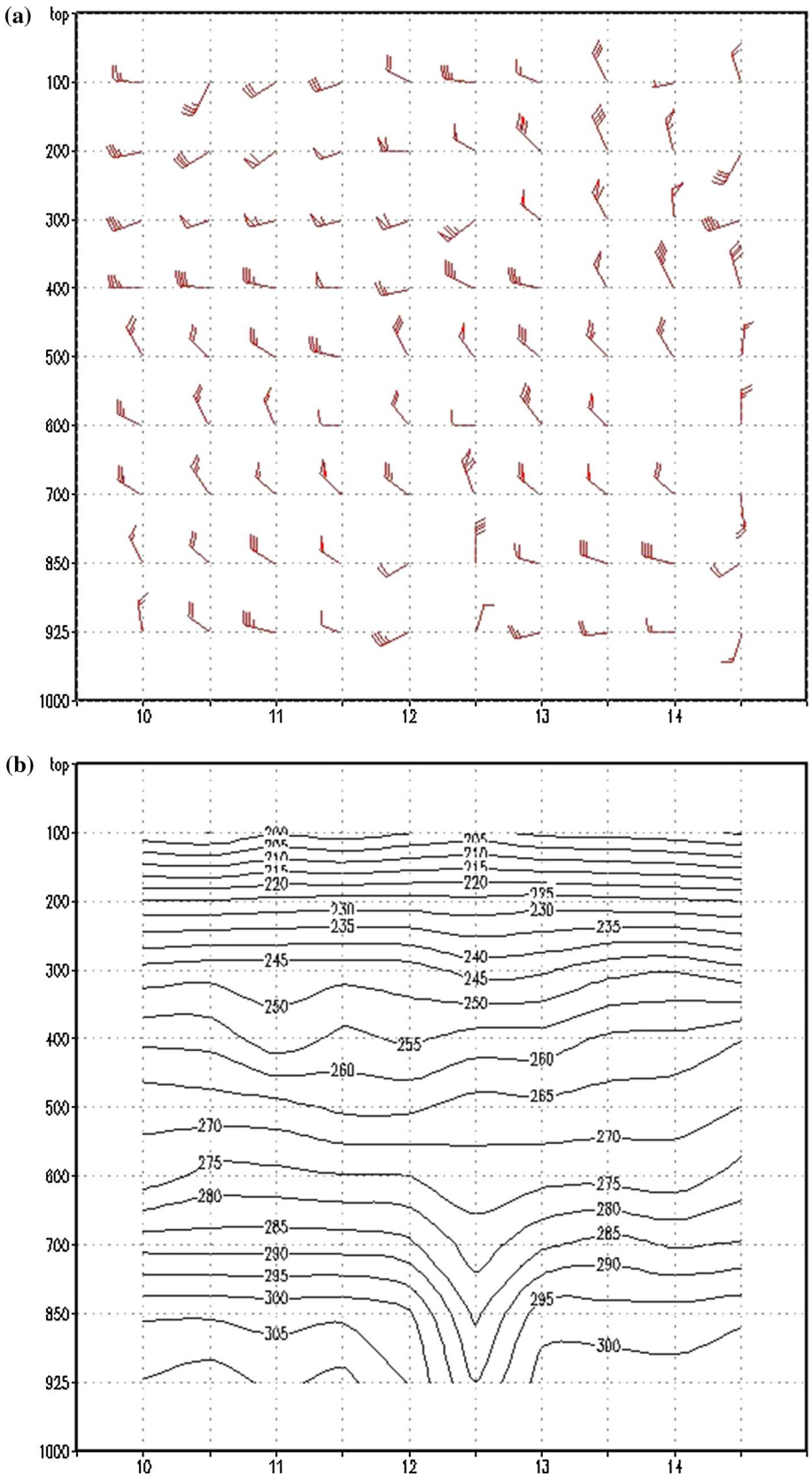

Fig. 13 Vertical profile of the **a** wind field (in knots) and **b** temperature (K in black contours), over Delhi during the period 10th June to 14th June 2014. For each day, two sets of observations at 0530 IST and 1730 IST are plotted in the same figure. *x*-axis denotes the date and *y*-axis is pressure levels in hPa

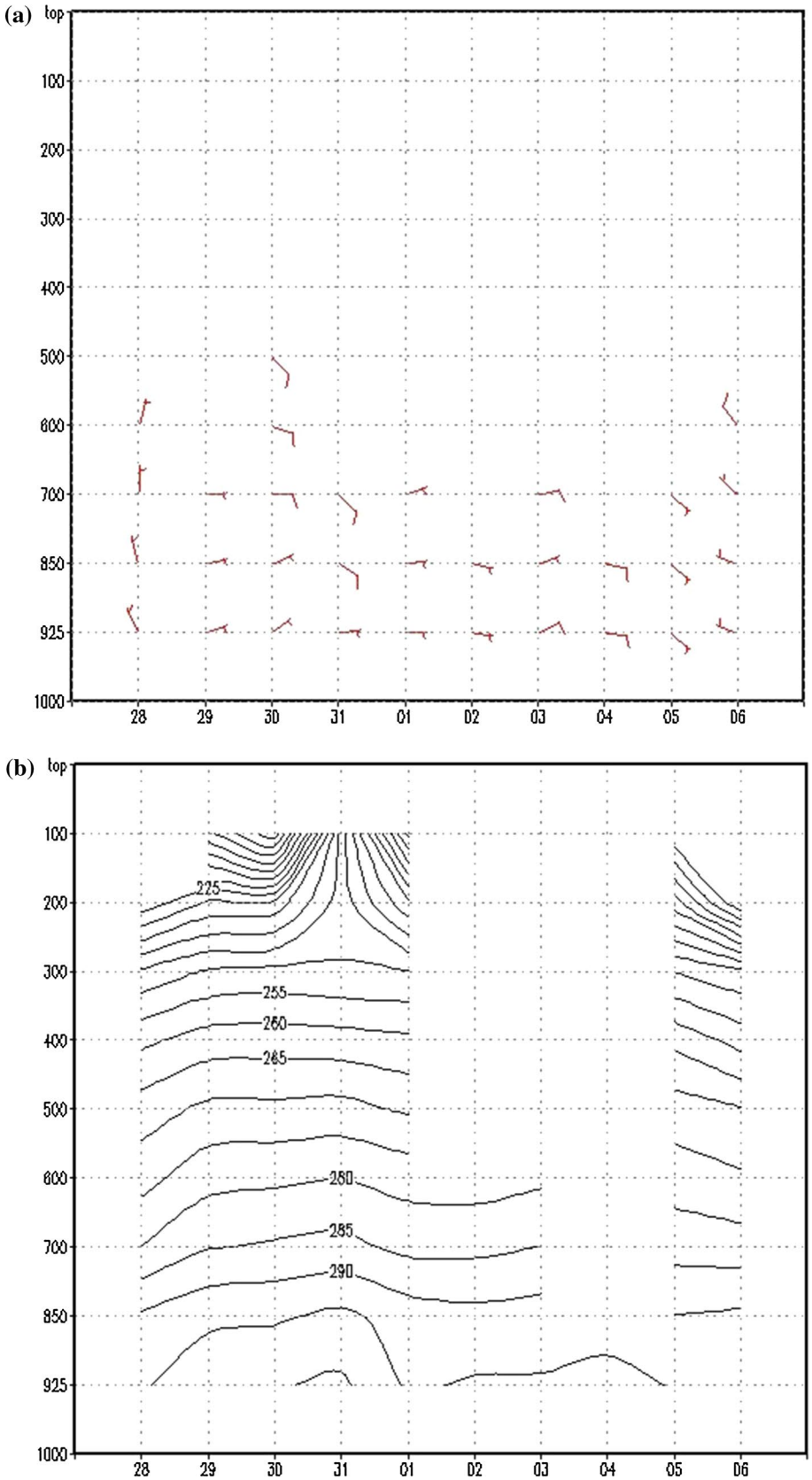

Fig. 14 Vertical profile of the **a** wind field (in knots) and **b** temperature field (K in black contours), over Delhi during the period 28th August to 06th September 2014. For each day, one set of observations at 0530 IST is plotted in the same figure. *x*-axis denotes the date and *y*-axis is pressure levels in hPa

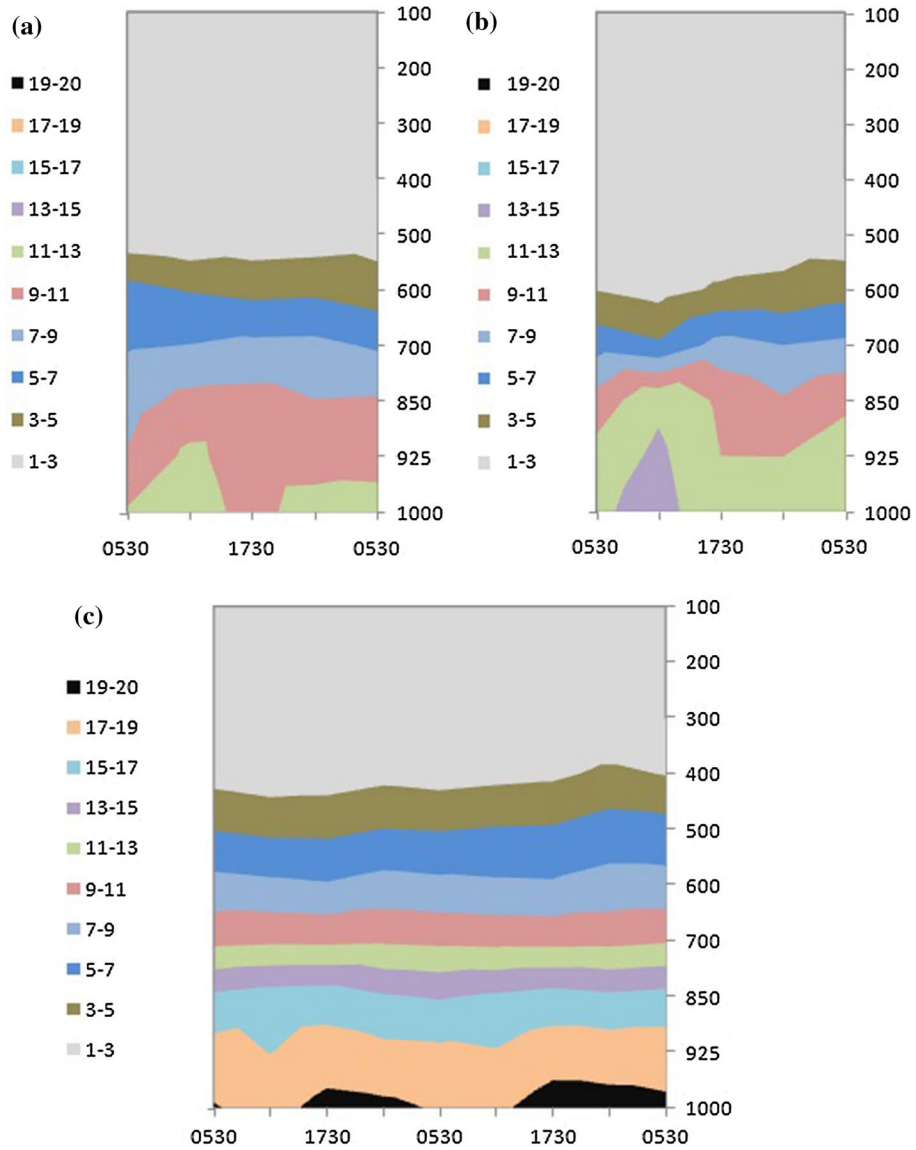

Fig. 15 Vertical profile of the ERA-Interim analysis specific humidity (in g/kg) averaged over the analysis domain of Delhi during the period **a** 0530 IST of 30th May to 0530 IST of 31st May 2014, **b** 0530 IST of 12th June to 0530 IST of 13th June 2014, and **c** 0530 IST of 03rd September to 0530 IST of 05th September 2014. For each day, four sets of reanalysis values are plotted in the same figure. *x*-axis denotes time and *y*-axis is pressure level in hPa

100°E as in Fig. 9d) along the foothills of the Himalayas. The cyclonic circulation subsequently moved away eastwards after 31st May. There was also a wind discontinuity to the west of Delhi at 925 hPa on both 30th and 31st May (as may be seen in Fig. 9d for 30th May 2014). While it appeared as a feeble discontinuity line in synoptic scale maps, it is significant since most of the weather systems appear to originate in situ over this region to the west of Delhi, before moving eastwards over to Delhi. This is also significant since the general pattern for most rainfall episodes occur over this region in association with the movement of westerly troughs, especially at the beginning of an episode. A sub-tropical westerly jet maximum was located further west over Afghanistan at 300 hPa (as may be seen in Fig. 9a for 30th May 2014) and aided the wind convergence over the North Indian region.

The time height cross-section of wind and temperature field from radiosonde data (Fig. 12a, b), indicated a strong diurnal cycle in the temperature field over the region. The temperature profile in the lower troposphere (below 850 hPa) showed a strong diurnal cycle and peak in the afternoon hours. While the model analysis field indicated a generally westerly wind field at lower levels (850 hPa and below) over the northwest Indian region throughout the event, the radiosonde data over the station indicated that the low-level wind field over the station (below 850 hPa) was more variable, with a southerly component in the wind field in the afternoon hours up to 31st May during the rainfall event over the domain. The wind was westerly aloft, and a strong northwesterly speed shear was seen over the station above 700 hPa on all the days up to 31st May, with wind speed increasing with height. However, on all

Table 1 Radar observation of the evolution of convection during the three episodes

Date	Time interval of observation (IST)	Organization of the cells with height of 20 dBZ echo top and maximum reflectivity and formation w. r. t radar station and direction of movement
29th May 2014	1430–1620	Isolated cells with intensity not exceeding 40 dBZ and cloud top height above 15 km formed about 350 km to the northeast of the radar. Stationary, short-lived cells formed on hilly terrain
30th May 2014	0550–1510	Isolated low-intensity cells with cloud top height about 15 km formed northwest of the radar moving eastwards towards the Himalayan foothills and intensifying in the hilly terrain in the morning hours. These later formed into convective zones further southwards and moved in southeasterly direction
	1520–2220	Intermittent organization of the convection region into a squall line (about 200 km long). The system crossed Delhi between 1630 and 1800 IST moving in a east-southeasterly direction. Cell height and intensity grew as the system moved eastwards with peak intensity of 60 dBZ and 50 dBZ contour crossing 17 km height. The squall line exits to the southeast sector of the radar (Fig. 16a, b). Convection ceases in the radar domain thereafter
31st May 2014	0130–0640	Isolated cells with intensity not exceeding 40 dBZ and cloud top height above 15 km formed about 50 km to the southwest of the radar and moved eastwards across the radar domain
11th June 2014	1010–2400	Two groups of isolated cells formed about 300 km to the northwest and south-southwest of the radar (intensity not exceeding 45 dBZ and cloud height of 20 dBZ contour about 15 km). They moved eastwards during the course of the day. The cells to the north of the radar intensified upon reaching the Himalayan foothills. The cells to the south of the radar reached peak intensity around 1630 IST and died down thereafter (Fig. 17a for 1630 IST of 11th June)
12th June 2014	1320–2400	Multiple isolated cells emerged around the same time, close to the radar. They later interacted to form larger convection lines oriented northwest–southeast along the direction of the southeasterly flow direction. Maximum intensity at about 1720 IST (Fig. 17b) with length about 500 km and about 150 km wide. Average maximum intensity about 50 dBZ and height of 20 dBZ contour < 15 km
13th June 2014	0000–2400	Convection increases up to about 0730 IST (Fig. 17c for 0740 IST) decreases to a minimum at around 1210 IST before increasing again. Character of convection the same as the previous day with convective lines oriented along the flow
02nd Sep 2014	0000–2400	Initially, isolated cells formed about 300 km to the north of the radar along the foothills of the Himalayas and then further south, closer to the radar. They increased in number after 1230 IST and moved from southeast to northwest direction across the radar. They gained intensity further to the northwest of the radar. Average cell height is about 10 km (20 dBZ contour) which increases to 15 km around 1730 IST (Fig. 18a) and decreased thereafter. Maximum reflectivity did not cross 40 dBZ
03rd Sep 2014	0000–2400	Isolated cells formed around the radar. These cells gained in intensity and organized into convective lines oriented along the flow from 1130 IST and moved from southeast to northwest direction. Average cell height was about 10 km (20 dBZ contour) which increases to 15 km around 1450 IST. Fresh cells form up to 1730 IST, but decrease thereafter. However, cell intensity does not increase beyond 40 dBZ (Fig. 18b at 1900 IST). While number of convective cells decreases thereafter, remnants of the cells persist
04th Sep 2014	0000–2400	Convection decreases from the previous day till 1730 IST, before increasing again. Initial direction of movement is from southeast to northwest and orientation of convective lines is likewise. However, from 1100 IST, the convection regions started to move in a northerly direction towards the Himalayan foothills. A long-lived convective line formed between 1900 IST and 2350 IST (Fig. 18c at 2300 IST). It was about 400 km long, oriented in a northwest-southeast direction and moved in a northerly direction across Delhi
05th Sep 2014	0000–2400	At about 0200 IST, fresh convection developed along the foothills of the Himalayas, to the northeast of the radar, moved southwestward during 0530 IST to 1100 IST, but died down before reaching Delhi. Fresh convection was also initiated to the southwest of the radar at 0530 IST, which later organized into a series of northwest–southeast oriented convective lines moving in a northerly direction across the station throughout the day (Fig. 18d at 1500 IST)

the days, the wind speed as well as the vertical shear was higher in the morning soundings at 0530 IST as compared to the afternoon sounding. The diurnal cycle of the specific humidity field as obtained from the ERA-Interim Reanalysis field (Fig. 15a) indicated that the lower atmospheric moisture peaks in the morning (at about 1130 IST), and lags the increase in the wind speed at all the levels in the morning sounding.

Radar observations for 29th–31st May 2014 are detailed in Table 1. As may be noted from the table, initial convection on 29th and 30th May was in the westerly flow, and was confined to the foothills of the Himalayas to the north of the radar, in the morning hours. There were no thunderstorm reports on 29th May. However, on 30th May, there were reports of thunderstorm occurrence from stations all over the Northern Himalayas to the north of the radar up to

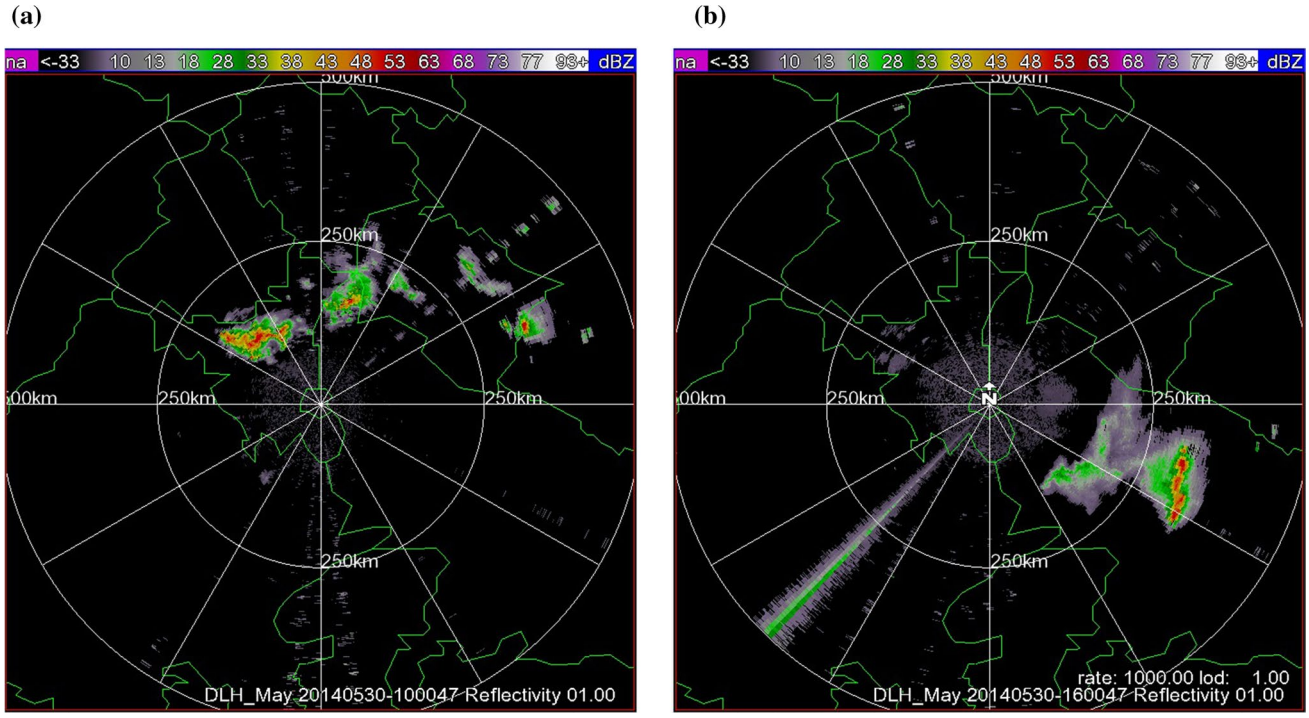

Fig. 16 Snapshots of radar reflectivity Plan Position Indicator (PPI) centred at Delhi at **a** 1530 IST and **b** 2130 IST of 30th May of a squall line mesoscale convective system which repeatedly formed and disorganized during the period

1100 IST. There were more reports from further south and the northwest Indian plains later in the day, including the plains to the west of Delhi. The convection formed later on that day moved in a southeasterly direction across the radar. Bluestein and Jain (1985) defined squall lines as mesoscale convective systems in which a system of mutually interacting cells forms on the boundary of fronts or dry lines, having a length to breadth ratio of 5:1, about 100 km long and with minimum lifetime of 15 min. They must also propagate perpendicular to the mean wind shear vector or mean steering flow. It was noted that a squall line repeatedly organized and disorganized over the domain between 1220 and 2230 IST of 30th May, with an average lifetime of 30–40 min (Fig. 16a, b for radar PPI snapshot of squall line mesoscale convective system at 1530 IST and 2130 IST of 30th May which disorganized within an hour of formation, before re-organizing at 1830 IST). These squall lines were much shorter (~ 100 km long), less organized (less clear convective cloud–stratiform cloud separation) and short lived (30–40 min) as compared to similar squall lines which formed later during the season which were more than 1000 km long, more organized and long lived (4–8 h lifetime). Wind squalls with speed of 115 km/h were reported when the squall line passed over Delhi between 1654 and 1703 IST. The convection died down in the radar domain by 0640 IST of 31st May. More thunderstorm reports were received from stations to the east of the radar station through the evening and night of 30th May and later, indicating southeastward shift in the main zone of convection.

The vertical reflectivity profiles for the 40 dBZ and 20 dBZ threshold isopleths (Fig. 5a, b) indicate that there was significant cloud cover over the domain between 1330 IST of 30th May and 0030 IST of the subsequent day. This was mostly convective, with maximum value between 1730 IST and 2030 IST and which was also the time when squall lines were seen in the radar domain. The cloud top at 40 dBZ reached 12 km while the 20 dBZ contour reached 15 km. The convection decreased thereafter, and was relatively cloud free around 0230 IST of 31st May and started increasing thereafter up to 0530 IST. The freezing level during the event was at about 4.8 km. Significant presence of stratiform clouds did not appear during the event. Rainfall maximum over the domain (Fig. 8a) coincided with the cloud maximum.

4.2 Case 2: (12–13 June 2014)

Although this case was only about 11 days following the preceding case, the synoptic features resulting in the rainfall were very different. Figure 10a–d displays the analysis maps of GFS model initialized at 0530 IST of 12th June 2014 for 300 hPa, 500 hPa, 850 hPa, and 925 hPa, respectively.

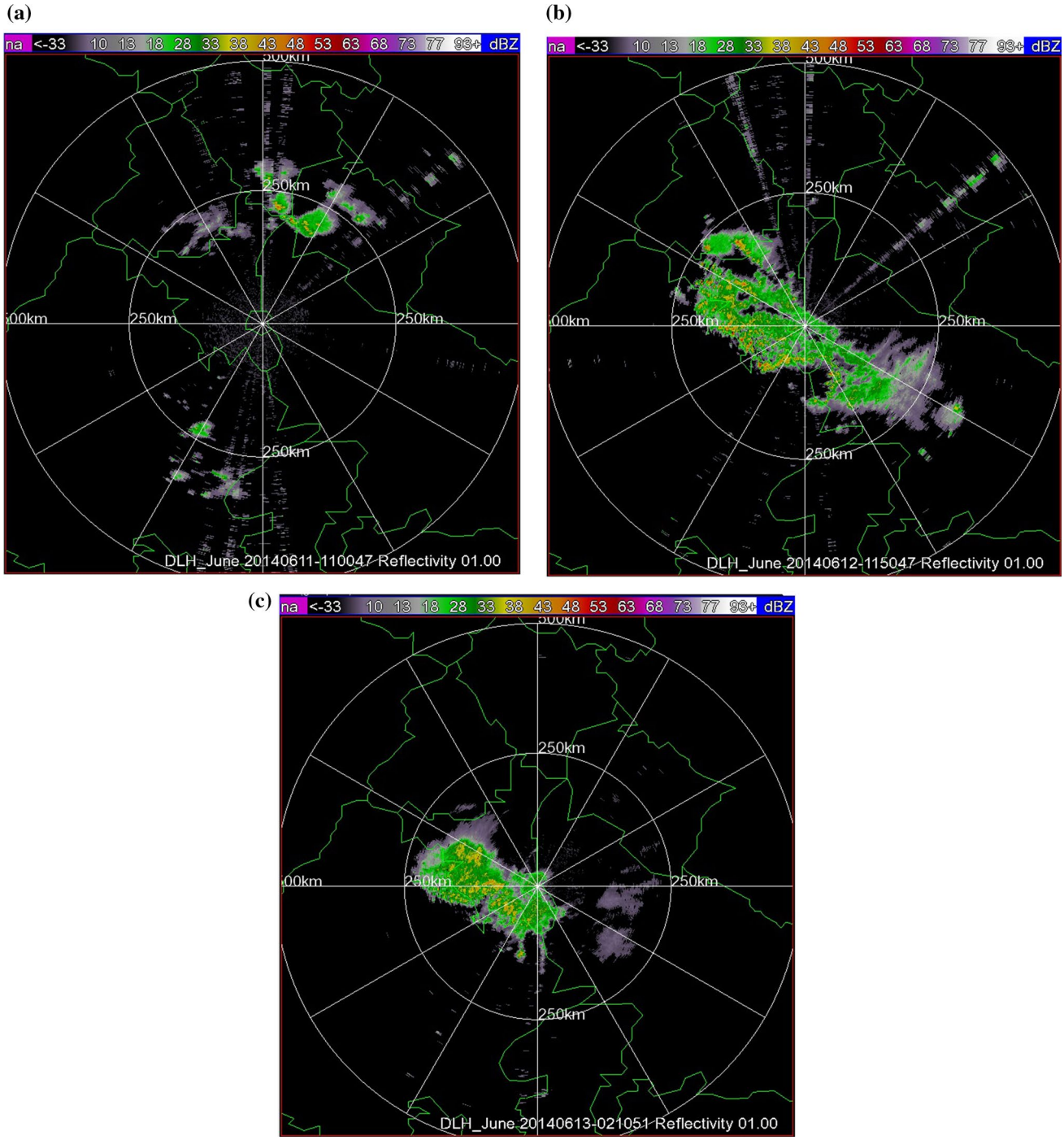

Fig. 17 Snapshots of radar reflectivity PPI centred at Delhi at **a** 1630 IST of 11th June, **b** 1720 IST of 12th June and **c** 0730 IST of 13th June of during the weather episode

Unlike the previous case, moisture incursion from the Arabian Sea into the northwest Indian sub-continental region started from 11th June in association with the cyclonic storm NANAUK over the Arabian Sea and along the edge of the anticyclone over North India. The sub-tropical westerly jet stream was present at 300 hPa with a jet core maximum over Pakistan, to the west of Delhi and there was associated low-level convergence over the region. However, unlike the previous case, there was no westerly trough in the middle troposphere over the region or an associated cyclonic

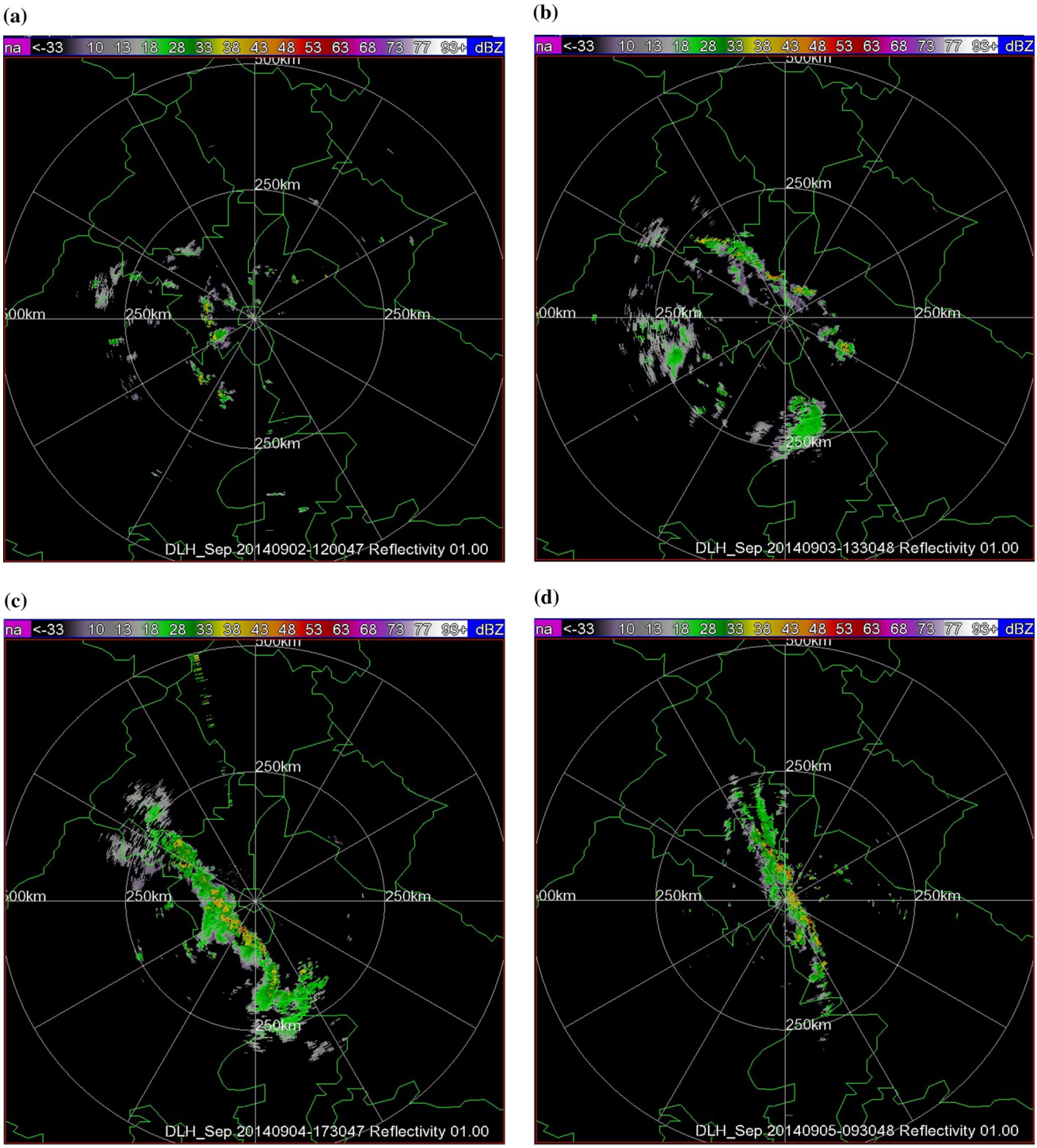

Fig. 18 Snapshots of radar reflectivity PPI centred at Delhi at **a** 1730 IST of 02nd September, **b** 1900 IST of 03rd September, **c** 2300 IST of 04th September and **d** 1500 IST of 05th September during the weather episode

circulation in the lower levels to promote convection. Analysis of radiosonde data indicated a strong diurnal cycle of variation in the temperature field, especially in the lower levels (Fig. 13a, b). The wind direction was variable throughout the period. However, although the southerly component in the wind field was stronger in the morning sounding, low-level vertical shear as well as wind speed (below 700 hPa) increased at 1730 IST soundings compared to the morning sounding. The shear values in the low-to-middle levels were generally comparable with the previous case. The diurnal

cycle of the specific humidity field as obtained from the ERA-Interim Reanalysis field (Fig. 15b) indicates that the lower atmospheric moisture peaks in the morning (at 1130 IST), and lags the increase in the wind speed at all levels in the morning sounding by about 6 h. However, since there was no organized convection (in the form of a squall line as in the previous case), the lifetime of the convection region was very short. Hence, the realized rainfall was less than the previous case.

Analysis of radar data and observations during 11th to 13th June is described in Table 1 and illustrated in (Fig. 17a–c). In brief, the initial convection on 11th June was in the form of isolated cells, which gained peak intensity at about 1630 IST (Fig. 17a). Thunderstorm reports were received from northwest Indian hills, to the north of the radar station, and to the west of the radar over Rajasthan between 1610 and 2400 IST. Organization of isolated cells into convection regions started on 12th June and continued on 13th June. Multiple groups of isolated cells were formed over the domain at 1320 IST of 12th June, and organized thereafter into convection regions which were oriented in a northwest–southeast direction, along the direction of their movement in a southeasterly direction. They reached peak intensity and organization about 3–4 h after the local noontime and a second maximum of convection occurred between 0030 and 0730 IST of 12th June before decreasing to a minimum at 1130 IST of 13th June and increasing thereafter. The subsequent convection of 13th June was a repeat of the convection of 12th June. Thunderstorm reports were more widespread throughout North India during the period, as compared to the previous case. They decreased on 13th June as compared to the previous day. However, there were no reports of severe squally or gusty winds over the region. The radar did not show any organization of the convection regions into squall lines.

The hourly accumulated reflectivity profile (Fig. 6a, b) indicates that large-scale convection appeared in the domain after 1430 IST of 12th June. The maximum values were observed at 1730 IST throughout the profile, indicating the period to be a primarily convective cloud regime. Thereafter, the maximum of both isopleths decreased, and appeared to concentrate around the 5 km freezing level. Pixel amounts (>20 dBZ as well as >40 dBZ isopleths) decreased after 0130 IST, while a second maximum appeared around the freezing level at 0230 IST. This indicated that stratiform clouds were more frequent in the domain after the 1730 IST convection maximum and also dominated the second peak at 0230 IST. As noted in the spatial pattern, the cells at the time of the latter peak of convection formed a large amorphous convection region with large stratiform outflows. The rainfall values (Fig. 8b) also indicated a large peak which was coincident with the convective cloud maximum. Another noteworthy fact about the case was the low cloud top height (10 km or less for both the 20 dBZ and 40 dBZ isopleths) of most clouds as compared to the previous case.

4.3 Case 3: (3–5 September 2014)

Two monsoon low-pressure systems formed over the Bay of Bengal and subsequently followed a northwestward track across the Indian subcontinent during the period of 27th August to 13th September. A third low-pressure area was formed on 02nd–04th September over the tip of Gujarat and the adjoining northeast Arabian Sea. Under the effect of these systems, an extended period of rainfall activity was noted over the domain around Delhi during the period of 26th August to 13th September (as indicated by the daily accumulated TRMM 3B42 data in Fig. 3). Radar data for 3 days during the event are analyzed in detail in this study during 03rd–05th September 2014. There was widespread rainfall in the domain through the 3 days, compared to the preceding and following days. Figure 11a–d displays the analysis maps of GFS model initialized at 0530 IST of 3rd September 2014 for 300 hPa, 500 hPa, 850 hPa, and 925 hPa, respectively. The weather charts indicate that the axis of east–west-oriented monsoon trough over the Indian subcontinent connects the centres of the low-pressure system over Gujarat to the low-pressure system over South Rajasthan and eastward into the Bay of Bengal (as may be seen in Fig. 11b–d for 03rd September 2014). There was deep moisture flow (up to 500 hPa) from the Arabian Sea and Bay of Bengal into the North Indian region along the northern edge of the monsoon low-pressure system. The vertical profile of wind field in Fig. 14a indicates that the lower atmospheric wind field was very weak, with minimal shear. In addition, since only one sounding was released per day during this period, the diurnal cycle of variation of the wind and temperature field could not be analyzed. However, the general wind field was easterly up to 700 hPa on all the days between 29th August and 05th September. The diurnal cycle of the specific humidity field from the ERA-Interim Reanalysis field (Fig. 15c) indicates that unlike the previous two cases, the lower atmospheric moisture peaks in the afternoon. The lagged peak in specific humidity, compared with the previous two cases, may be due to the afternoon deepening of the monsoon low-pressure system, (in phase with the peaking of the surface sensible heating), that is responsible for pulling moisture into this region.

Table 1 gives a detailed analysis of the convection over the domain as observed in radar data while Fig. 11a–d illustrate the important features. Radar data (Fig. 18a–d) reveal that there was convection in the domain throughout the period, which generally moved in a westward direction. Convection was minimum in the morning on 2nd and 3rd September and started to build up after 1130 IST. Widespread light to moderate rainfall (51 mm max.) was reported across

North India on 2nd September, which increased thereafter. On 4th and 5th September, pre-existing convection continued from the previous day. Organized convection was in the form of convective lines, and convection generally increases on all the days up to about 1730 IST. While on 2nd and 3rd September, the convection decreased thereafter. On the night of 4th September, the convection persisted, and in fact gained intensity at about 0230 IST of the next day. Convection also originated along the foothills of the Himalayas at night around 0200 IST of 4th September, to the northeast of the radar station, which moved in a southerly direction towards the radar station. This increase in convection was accompanied by an increase in the spread and intensity of the rainfall reported by observing stations (101 mm max. rainfall reported on 4th September and 218 mm max. rainfall reported on 5th September).

The hourly accumulated reflectivity pixel profile (Fig. 7a, b) indicates that large-scale convection was initiated over the domain from 1430 IST of 03rd September and peaked at 1730 IST. Although the lower tropospheric moisture was higher than the two previous events, the > 40 dBZ reflectivity values did not cross 8 km; although the > 20 dBZ isopleths reach up to 12 km. In addition, while on 03rd September there was only one reflectivity maximum centred at 1730 IST, on 04th September, there was a bimodal reflectivity maximum, with twin maxima at 1730 IST and 0230 IST. In addition, unlike the previous case, the second peak at 0230 IST was not a stratiform maximum. The spatially accumulated 3-hourly rainfall from TRMM data (Fig. 8c) showed a peak value of rainfall at 1730 IST of 03rd September and a weak second peak at 0230 IST. However, on 04th September, the second peak at 0230 IST predominated.

5 Discussion and conclusions

Delhi, in common with most of the North Indian subcontinent, has two major weather regimes—monsoon and non-monsoon seasons. As representative of the general atmospheric conditions over the region, this analysis concentrates on two types of atmospheric conditions—(a) moderate vertical shear (between 4 and 10 m/s) with low precipitable water content (< 40 mm) conditions (cases 1 and 2), which are typical of pre-monsoon weather and (b) low wind shear (< 2 m/s) with high precipitable water content (> 60 mm) (case 3) which is representative of monsoon weather. Cases 1 and 2 differ in that, on the days of convection, the environment was characterized by unidirectional shear for case 1 (above 850 hPa), and directionally varying shear for case 2.

Weisman and Klemp (1982, 1984) noted that over the United States, single-cell weather systems preferentially formed in low vertical wind shear environment while moderate vertical wind shear (< 15 m/s) favoured the formation of multicellular weather systems. In addition, higher CAPE values (> 2000 J/kg) with low wind shear environment favoured the formation of multicellular thunderstorm systems. High wind shear conditions (> 15 m/s) (multidirectional or unidirectional) increased the probable formation of super cells. Over the Delhi region, wind shear values of the atmosphere during these rainfall episodes (computed by the same method) were generally very low (< 14 m/s as in Fig. 4). Correspondingly, there are very few historical records of super cell formation over this region. In line with the findings of Weisman and Klemp (1982, 1984), multicellular convection zones prevailed during the entire period of convection for all three cases throughout the domain. It was noted that fresh convection was in the form of isolated cells which were mostly initiated during the morning hours, in phase with the building up of moisture in the atmosphere. Multicell thunderstorms developed later in the afternoon. The most common type of mesoscale organization of the clouds in all the three cases was in the form of convective lines. These lines generally move along the mean steering flow of the lower troposphere. Cases 1 and 2 were characterized by short bursts of convection throughout the observation period, with short-lived convection zones comprising of taller cells (20 dBZ contour at about 15 km) as compared to case 3 (20 dBZ contour at about 10 km). The cell height and width (about 10 km on an average) were generally similar for cases 1 and 2 (except during the period of 1520–2120 IST of 30th May for case 1, when the clouds were organized into a squall line system and cells were taller ~ 20 km and longer lived). The consistent anti-correlation of cell width with cell height observed in the three cases may be ascribed to the downward Buoyancy Pressure-Gradient Acceleration field (BPGA) in the cells which oppose the buoyancy due to sensible and latent heat of the rising parcel. It increases as the cell width increases, and limits the growth of broader cells more than narrower cells (Houze 2014). The cells in the convection zones had the least stratiform outflow for case 1, more stratiform outflow for case 2 and longest lifetimes and broadest cells (about 30–40 km on average) for case 3. Consequently, the convection zones were smallest in case 1, larger for case 2 and largest in case 3.

An analysis of multiple cases of squall line formation over the region during this season indicates the importance of unidirectional shear in triggering the formation of squall lines similar to those in case 1. Since squall lines over the region are generally associated with most severe surface winds, this may explain the climatological predominance of severe squally winds during the pre-monsoon season (March

to May), when these atmospheric conditions are mostly predominant (Ram and Mohapatra 2012).

Our analysis also indicates that the primary peak of convection and associated rainfall over the northwest Indian region, irrespective of the season, is in the afternoon hours between 1730 and 2030 IST, and lags the diurnal temperature maximum (around 1430 IST) by 3–5 h. This primary peak is essentially convective, and is associated with the gradual increase in the spatial scale of the convection region, which is actually initiated much earlier, in phase with the diurnal maximum of surface temperature. When there is sufficient moisture in the atmosphere, a second peak in convection and associated rainfall appears over the region, during the early morning hours (between 0230 and 0530 IST). This peak has a greater fraction of stratiform clouds at the beginning of an episode, but the convective fraction and the rainfall peak increases on day 2 or later into a multiday episode, as the moisture builds up in the atmosphere.

As discussed in the introduction, satellite-based observations of the diurnal evolution of cloud cover have also noted that mesoscale convection tended to result in a late afternoon maximum, while deep organized convection peaks in early morning (Laing and Fritsch 1997; Romatschke et al. 2010; Sui et al. 1997). Some studies have hypothesized that this early morning peak in convection over land regions is analogous to the oceanic "Static Radiation-Convection" (SRC) (Dai 2001). This is a synoptic scale mechanism that presumes that enhanced cloud top infrared cooling at night, stemming from the lack of cloud top solar absorption, and a consequent increase in the thermal lapse rate favour more intense rainfall during the late night period, provided there is a pre-existence of cloudiness. Other studies of arid and semi-arid areas have noted that the winds are at their weakest in the afternoon when the convective boundary layer is deep and temperature is maximum and intensify overnight when the boundary layer turbulence is much weaker (Parker et al. 2005). This causes diurnal maximum intensity of the low-level pressure field in the early morning, resulting in an early morning peak in convection in the presence of adequate moisture. Deshpande and Goswami (2014) observed that, over Central India during the active phase of monsoon season, an early morning reduction in geopotential height and increase in specific humidity of 850 hPa is in phase with the early morning maximum of rainfall which supports the latter findings.

The diurnal cycle of the specific humidity field in our study for the first two of the three cases, as obtained from the ERA-Interim Reanalysis field indicate that the lower atmospheric moisture peaked during early morning (Fig. 15a–c), and in the afternoon for the case 3. In all the three cases, the maximum convection lags the diurnal maximum of moisture indicating other factors, such as the sensible heat cycle at play to produce the afternoon convection maximum. The SRC mechanism may primarily be responsible for the late night-early morning maximum, especially for long-lived MCS. Earlier studies have also noted that the enhancement of large systems in the Himalayan foothills in the morning supports the hypothesis of dynamic pressure deceleration (Barros and Lang 2003). Our observations indicate that these systems that form over the Himalayas are not a necessary factor in the early morning peak in rainfall and convection over the Delhi region.

This also implies that pre-monsoon convection over Delhi is primarily unimodal, its maximum amount lagging the diurnal moisture maximum, and to a lesser extent the diurnal temperature maximum as well. It is characterized by short bursts of intense convection with narrow and short-lived cells. Monsoon convection on the other hand, is essentially bimodal, with the early morning peak, often pre-dominating over the afternoon peak, especially for long-lived weather systems with more moisture in the atmosphere. It is characterized by longer lived cells which are less intense than cells of the pre-monsoon weather systems.

Acknowledgements The authors would like to acknowledge helpful guidance of Dr. Mike Dixon at NCAR RAL (USA), for developing program to convert Delhi radar data in cfradial netcdf format and subsequently providing the "Radx" application for Cartesian conversion. The authors are also grateful to the Director General of Meteorology, India Meteorological Department, for constant encouragement during the course of this study. We are grateful to a large number of colleagues in Radar Division and NWP Division of India Meteorological Department, New Delhi. We also acknowledge the use of TRMM rainfall data from NASA Tropical Rainfall Measuring Mission's Goddard Earth Sciences Data and Information Services Center (GESDISC) and radiosonde data from the University of Wyoming website http://weather.uwyo.edu/upperair/sounding.html.

References

Barros AP, Lang TJ (2003) Monitoring the monsoon in the Himalayas: observations in central Nepal, June 2001. Mon Weather Rev 131(7):1408–1427

Basu BK (2007) Diurnal variation in precipitation over india during the summer monsoon season: observed and model predicted. Mon Weather Rev 135:2155–2167

Bhalotra YPR (1954) Statistical facts about squalls at Delhi. Mausam 5(4):551–555

Bhattacharya A, Chakraborty A, Venugopal V (2017) Role of aerosols in modulating cloud properties during active–break cycle of Indian summer monsoon. ClimateDyn 49(5–6):2131–2145. https://doi.org/10.1007/s00382-016-3437-4

Bluestein HB, Jain MH (1985) Formation of mesoscale lines of precipitation: severe squall lines in Oklahoma during the spring. J Atmos Sci 42(16):1711–1732

Chatterjee RN, Prakash P (1986) A radar study on the frequency of occurrence of cumulonimbus clouds around Delhi. Mausam 37(2):241–244

Churchill Dean D, Houze RA Jr (1984) Development and structure of winter monsoon cloud clusters on 10 December 1978. J Atmos Sci 41(6):933–960

Dai A (2001) Global precipitation and thunderstorm frequencies. Part II: Diurnal variations. J Clim 14:1112–1128. https://doi.org/10.1175/1520-0442(2001)014%3c1112:GPATFP%3e2.0.CO;2

Dai A, Giorgi F, Trenberth KE (1999) Observed and model simulated precipitation diurnal cycle over the contiguous United States. J Geophys Res 104:6377–6402

Davis C, Brown B, Bullock R (2006) Object-based verification of precipitation forecasts. Part I: Methodology and application to mesoscale rain areas. Mon Weather Rev 134(7):1772–1784

Dee DP, Uppala SM, Simmons AJ, Berrisford P, Poli P, Kobayashi S, Andrae U, Balmaseda MA, Balsamo G, Bauer P, Bechtold P, Beljaars ACM, van de Berg L, Bidlot J, Bormann N, Delsol C, Dragani R, Fuentes M, Geer AJ, Haimberger L, Healy SB, Hersbach H, Hólm EV, Isaksen L, Kållberg P, Köhler M, Matricardi M, McNally AP, Monge-Sanz BM, Morcrette JJ, Park BK, Peubey C, de Rosnay P, Tavolato C, Thépaut JN, Vitart F (2011) The ERA-Interim reanalysis: configuration and performance of the data assimilation system. Q J R Meteorol Soc 137:553–597. https://doi.org/10.1002/qj.828

Deshpande NR, Goswami BN (2014) Modulation of the diurnal cycle of rainfall over India by intraseasonal variations of Indian summer monsoon. Int J Climatol 34:793–807. https://doi.org/10.1002/joc.3719

Durai VR, Roy Bhowmik SK (2013) Prediction of Indian summer monsoon in short to medium range time scale with high resolution global forecast system (GFS) T574 and T382. Clim Dyn 42(5–6):1527–1551

Giorgi F, Mearns LO (1999) Introduction to special section: regional climate modeling revisited. J Geophys Res Atmos (1984–2012) 104(D6):6335–6352

Houze RA Jr (1997) Stratiform precipitation in regions of convection: a meteorological paradox? Bull Am Meteorol Soc 78(10):2179–2196

Houze RA Jr (2014) Basic cumulus dynamics. Cloud dynamics, vol 104. Academic Press, Waltham, pp 166–167

Houze RA Jr, Biggerstaff MI, Rutledge SA, Smull BF (1989) Interpretation of Doppler weather radar displays of midlatitudemesoscale convective systems. Bull Am Meteorol Soc 70(6):608–619

Houze RA Jr, Wilton DC, Smull BF (2007) Monsoon convection in the Himalayan region as seen by the TRMM precipitation radar. Q J R Meteorol Soc 133(627):1389–1411

Huffman GJ, Adler RF, Bolvin DT, Gu G, Nelkin EJ, Bowman KP, Hong Y, Stocker EF, Wolff DB (2007) The TRMM multisatellite precipitation analysis (TMPA): quasi-global, multiyear, combined-sensor precipitation estimates at fine scales. J Hydrometeorol 8:38–55. https://doi.org/10.1175/JHM560.1

Laing AG, Fritsch JM (1997) The global population of mesoscale convective complexes. Q J R Meteorol Soc 123(538):389–405

Laurent H, Machado LAT, Morales CA, Durieux L (2002) Characteristics of the Amazonian mesoscale convective systems observed from satellite and radar during the WETAMC/LBA experiment. J Geophys Res 107(D20):8054. https://doi.org/10.1029/2001JD000337

Lin X, Randall DA, Fowler LD (2000) Diurnal variability of the hydrologic cycle and radiative fluxes: comparisons between observations and a GCM. J Clim 13(23):4159–4179

Maddox RA (1980) Mesoscale convective complexes. Bull Am Meteorol Soc 61:1374–1387

Maddox RA, Zhang J, Gourley JJ, Howard KW (2002) weather radar coverage over the contiguous United States. Weather Forecast 17:927–934. https://doi.org/10.1175/1520-0434(2002)017%3c0927:WRCOTC%3e2.0.CO;2

Marshall JS, Palmer WM (1948) The distribution of raindrops with size. J Meteor 5:165–166. https://doi.org/10.1175/1520-0469(1948)005%3c0165:TDORWS%3e2.0.CO;2

Mohr CG, Vaughan RL (1979) An economical procedure for Cartesian interpolation and display of reflectivity data in three-dimensionsal space. J Appl Meteorol 18:661–670

Mohr CG, Miller LJ, Vaughan RL (1981) An interactive software package for the rectification of radar data to three-dimensional Cartesian coordinates. Preprints 20th Conf. on radar meteorology, Boston, Am Meteorol Soc, pp 690–695

Nair S, Srinivasan G, Nemani R (2009) Evaluation of multi-satellite TRMM derived rainfall estimates over a Western State of India. J Meteorol Soc Jpn 87:927–939. https://doi.org/10.2151/jmsj.87.927

Nesbitt SW, Zipser EJ (2003) The diurnal cycle of rainfall and convective intensity according to three years of TRMM measurements. J Clim 16(10):1456–1475

Parker DJ, Burton RR, Diongue-Niang A, Ellis RJ, Felton M, Taylor CM, Thorncroft CD, Bessemoulin P, Tompkins AM (2005) The diurnal cycle of the West African monsoon circulation. Q J R Meteorol Soc 131(611):2839–2860

Peel MC, Finlayson BL, McMahon TA (2007) Updated world map of the Köppen–Geiger climate classification. Hydrol Earth Syst Sci Discuss 4(2):439–473

Puranik DM, Karekar RN (2009) Western disturbances seen with AMSU-B and infrared sensors. J Earth Syst Sci 118(1):27–39

Rahman SH, Sengupta D, Ravichandran M (2009) Variability of Indian summer monsoon rainfall in daily data from gauge and satellite. J Geophys Res 114:D17113. https://doi.org/10.1029/2008JD011694

Ram S, Mohapatra M (2012) Some aspects of Squall over Indira Gandhi International Airport, New Delhi. Mausam 63(4):623–638

Randall D, Krueger S, Bretherton C, Curry J, Duynkerke P, Moncrieff M, Ryan B, Starr D, Miller M, Rossow W, Tselioudis G (2003) Confronting models with data: the GEWEX cloud systems study. Bull Am Meteorol Soc 84(4):455–469

Rao YP, Srinivasan V (1968) Climatology of India and neighbourhood, 2: climate of India, FMU Report No. I-2, India Meteorological Department Forecasting Manual, New Delhi

Romatschke U, Houze RA Jr (2011a) Characteristics of precipitating convective systems in the premonsoon season of South Asia. J Hydrometeorol 12:157–180. https://doi.org/10.1175/2010JHM1311.1

Romatschke U, Houze RA Jr (2011b) Characteristics of precipitating convective systems in the South Asian monsoon. J Hydrometeorol 12(1):3–26

Romatschke U, Medina S, Houze RA Jr (2010) Regional, seasonal, and diurnal variations of extreme convection in the South Asian Region. J Clim 23:419–439. https://doi.org/10.1175/2009JCLI3140.1

Roy Bhowmik SK, Sen Roy S, Srivastava K, Mukhopadhay B, Thampi SB, Reddy YK, Singh H, Venkateswarlu S, Adhikary S (2011) Processing of Indian Doppler Weather Radar data for mesoscale applications. Meteorol Atmos Phys 111(3–4):133–147

Schiemann R, Lüthi D, Schär C (2009) Seasonality and interannual variability of the westerly jet in the Tibetan Plateau region. J Clim 22(11):2940–2957

Sen Roy S, Sen Roy S (2011) Regional variability of convection over northern India during the pre-monsoon season. Theor Appl Clim 103(1–2):145–158. https://doi.org/10.1007/s00704-010-0289-4

Sen Roy S, Sen Roy S (2014) Diurnal variation in the initiation of rainfall over the Indian subcontinent during two different monsoon seasons of 2008 and 2009. Theor Appl Clim 117(1):277–291. https://doi.org/10.1007/s00704-013-1006-x

Sen Roy S, Saha SB, Roy Bhowmik SK, Kundu PK (2014) Optimization of Nowcast Software WDSS-II for operational application

over the Indian region. Meteorol Atmos Phys 124(3):143–166. https://doi.org/10.1007/s00703-014-0315-7

Sen Roy S, Saha SB, Roy Bhowmik SK, Kundu PK (2015) Diurnal cycle of rainfall as predicted by WRF model: verification using model evaluation tools software. Mausam 66(3):349–360

Serafin RJ, Wilson JW (2000) Operational weather radar in the United States: progress and opportunity. Bull Am Meteorol Soc 81:501–518. https://doi.org/10.1175/1520-0477(2000)081%3c0501:OWRITU%3e2.3.CO;2

Shige S, Nakano Y, Yamamoto MK (2017) Role of orography, diurnal cycle, and intraseasonal oscillation in summer monsoon rainfall over Western Ghats and Myanmar coast. J Clim. https://doi.org/10.1175/JCLI-D-16-0858.1

Steiner M, Houze RA Jr, Yuter SE (1995) Climatological characterization of three-dimensional storm structure from operational radar and rain gauge data. J Appl Meteorol 34:1978–2007

Sui CH, Lau KM, Takayabu YN, Short DA (1997) Diurnal variations in tropical oceanic cumulus convection during TOGA COARE. J Atmos Sci 54:639–655

Tokay A, Short DA (1996) Evidence from tropical raindrop spectra of the origin of rain from stratiform versus convective clouds. J Appl Meteorol 35:355–371

Trenberth KE, Fasullo JT (2010) Tracking Earth's energy. Science 328(5976):316–317

Trenberth KE, Fasullo JT, Kiehl J (2009) Earth's global energy budget. Bull Am Meteorol Soc 90(3):311–323

Weisman ML, Klemp JB (1982) The dependence of numerically simulated convective storms on vertical wind shear and buoyancy. Mon Weather Rev 110(6):504–520

Weisman ML, Klemp JB (1984) The structure and classification of numerically simulated convective stormsin directionally varying wind shears. Natl Center Atmos Res 112:2479–2498. https://doi.org/10.1175/1520-0493(1984)112%3c2479:TSACON%3e2.0.CO;2

Yang GY, Slingo J (2001) The diurnal cycle in the tropics. Mon Weather Rev 129:784–801. https://doi.org/10.1175/1520-0493(2001)129%3c0784:TDCITT%3e2.0.CO;2

Yang S, Smith EA (2008) Convective-stratiform precipitation variability at seasonal scale from 8 years of TRMM observations: implications for multiple modes of diurnal variability. J Clim 21:4087–4114. https://doi.org/10.1175/2008JCLI2096.1

Yuter SE, Houze RA Jr (1995) Three dimensional kinematic and microphysical evolution of Florida cumulonimbus. Part III: vertical mass transport, mass divergence and synthesis. Mon Weather Rev 123:1964–1983